2011

SELECTIVE TRANSLOCATION OF CELL-IMPERMEABLE TOXINS INTO CANCER CELLS: pHLIP MEDIATED DELIVERY OF PHALLOTOXINS INHIBITS CANCER PROLIFERATION

Dayanjali Diluka Wijesinghe
University of Rhode Island, diluka@my.uri.edu

SELECTIVE TRANSLOCATION OF CELL-IMPERMEABLE TOXINS INTO CANCER CELLS: pHLIP MEDIATED DELIVERY OF PHALLOTOXINS INHIBITS CANCER PROLIFERATION

BY

DAYANJALI DILUKA WIJESINGHE

A DISSERTATION SUBMITTED IN PARTIAL FULFILLMENT OF THE REQUIREMENTS FOR THE DEGREE OF

DOCTOR OF PHILOSOPHY

IN

PHYSICS

UNIVERSITY OF RHODE ISLAND

2011

DOCTOR OF PHILOSOPHY DISSERTATION

OF

DAYANJALI DILUKA WIJESINGHE

APPROVED:

Thesis Committee:

Major Professor Yana Reshetnyak

Oleg Andreev

Brenton Deboef

Bongsup Cho

Nasser Zawia
DEAN OF THE GRADUATE SCHOOL

UNIVERSITY OF RHODE ISLAND
2011

ABSTRACT

Most drug molecules cannot freely diffuse across a cellular membrane because of the energetic barrier for transition across a hydrophobic lipid bilayer of a membrane is very high for polar molecules. Recently it was discovered that a moderately hydrophobic, water-soluble membrane peptide called pHLIP® (pH (Low) Insertion Peptide) can insert into membranes and translocate molecules in a pH-dependent manner. This opens aunique opportunity to develop a novel concept in drug delivery, which is based on the use of a pH-sensitive single peptide molecular transporter. The main goal of this investigation is to elucidate mechanism of cargo translocation across a membrane by the single molecule transporter, pHLIP, and to demonstrate its utility for the translocation of function cargo molecules. We have carried out a variety of biophysical experiments and investigation on the cultured cells. As a functional cargo we selected a cyclic cell-impermeable polar peptide, phallatoxin (phalloidin or phallacidin) from the deadly *Amanita phalloides* mushroom. If it is delivered into a cell, it would bind tightly to actin filaments at nanomolar concentration and inhibits their depolymerization. Previously our lab has demonstrated that the pHLIP is capable of translocation of phalloidin-rhodamine across a cellular membrane. In the present study, we show that the pHLIP can move phalloidin across the membrane, when the hydrophobic facilitator (rhodamine) was attached to the peptide inserting end. The phalloidin translocated across a cellular membrane by the pHLIP induces > 90% inhibition of HeLa, JC and M4A4 cancer cell growth, their cytoskeletal immobilization and multinucleation, consistent with the expected binding of phalloidin to F-actin. The next step of our studies was tuning the hydrophobicity of

polar cargo. We designed, synthesize and characterize three phallacidin cargoes, where the hydrophobicity of cargo was tuned by the attachment of diamines of different lengths of hydrophobic chains. The phallacidin cargo (phallC6) with a similar polarity to phallodin-rhodamine was conjugated to the pHLIP, and shown to selectively inhibit the proliferation of cancer cells at low pH. To elucidate the mechanism of cargo translocation across a membrane by the pHLIP and identify pHLIP variants for more efficient molecules translocation across a membrane, we carried out biophysical studies on several pHLIP variants conjugated with the cargoes of different polarity (biotin and biotin-Peg). We confirm that all pHLIP variants with attached cargo molecules preserve pH-dependent properties of interaction with membrane. While the equilibrium thermodynamics favor the binding and insertion of pHLIP-cargo constructs, kinetics was significantly slowed down. Our findings are valuable for the design of new delivery agents for the direct translocation of polar cargo across a membrane: to facilitate the different delivery needs for different applications the hydrophobicity of the cargo could be modified without affecting cargo's ability to bind to its cellular target and/or various peptides of the pHLIP family could be employed, which show different rates and pKa of the cargo translocation across cellular membranes. Thus, the maximum difference between the therapeutic effects at low pH versus at neutral pH could be achieved, thereby enhancing diseased-targeted delivery and reducing treatment side effects.

ACKNOWLEDGMENTS

This dissertation would not have been possible without the guidance and support of several individuals who in different ways extended their valuble assistance to preparation and completion of this study. First and formost, I owe my deepest gratitude to my major professor Dr. Yana Reshetnyak for her immense support, encouragement, understanding and patience throughout my research mainly when I hurdle many obstacles. It was a great honor and privilege to work under your supervision where I gained broad research skills, analysis techniques and furthermore was reminded to approach a problem with clarity of thoughts. Next, I am heartily thankful to Dr. Oleg Andreev for your valuable insights and guidance throughout my dissertation research. I would also like to thank Dr. Brenton Deboef for his valuable time, discussions related to chemical conjugations and granting generous access to his lab when needed. Also thank you Dr. Shathaverdhan Potavatri for the guidance in chemical reactions. I deeply thank Dr. Ming An for your guidance and valuable discussions in optimizing chemical reactions and Dr. Gregory Watkins for the insights in chemical experiments. Also my gratitude goes to Dr. Anna Moshnikova for the help and discussions with cell experiments and Erin Jansen for time consuming HPLC purifications. I also thank all my colleagues specially Alexander Karabadzak and Dr. Lan Yao for discussions.

I thank my family, my dear husband Dhammika Weerakkody for his support when needed both as a colleague and a husband and my little darlings Dewni and Maneka for bearing with me. I greatly appreciate your understanding my ‘chooti doo’ Dewni, when you wanted me to spend more time with you but when I had to go to work. Last

but not least, I am greatly indebted to my parents for sacrificing their own comfort and wishes in order to take care of my very mischievous little ones. Thaththi, (dad) I am forever indebted to you for every day and night you had to stay away from ammi (mom) and for every minute you had to ‘put up’ with my darlings’ bad behavior. I have felt selfish many times for pursing my goals when many had to suffer but you ammi and thaththi made me kept going. I simply cannot thank you enough.

PREFACE

This dissertation is written in the 'Manuscript Fromat' using the Thesis/ Dissertation template of University of Rhode Island. There are three manuscripts, each organized into a chapter. Tables and figures of each manuscript are listed under the corresponding chapter in the list of tables and figures.

TABLE OF CONTENTS

LIST OF TABLES

LIST OF FIGURES

CHAPTER 3

CHAPTER 1

Published in Proceedings of National Academy of Sciences (PNAS) on 27th of Spetember, 2010

BIOLOGICAL SCIENCES: Applied Biological Sciences

Translocating Membrane-impermeable Toxins into Cancer Cells: pHLIP-mediated Delivery of Phalloidin Inhibits Cell Proliferation

Ming An[a], Dayanjali Wijesinghe[b], Oleg A. Andreev[b], Yana K. Reshetnyak[b], and Donald M. Engelman[a]

[a]Department of Molecular Biophysics and Biochemistry, Yale University, P.O. Box 208114, New Haven, CT 06520, USA

[b]Physics Department, University of Rhode Island, 2 Lippitt Rd., Kingston, RI, 02881, USA

Corresponding Authors:

Donald M. Engelman, Department of Molecular Biophysics and Biochemistry, Yale University, P.O. Box 208114, New Haven, CT 06520, USA, Phone: (203)-432-5601; Fax: (203) 432-6381, E-mail: donald.engelman@yale.edu

Yana K. Reshetnyak, Physics Department, University of Rhode Island, 2 Lippitt Rd., Kingston, RI, 02881, USA, Phone: (401)-874-2060, Fax: (401) 874-2380, E-mail: reshetnyak@mail.uri.edu

Oleg A. Andreev, Physics Department, University of Rhode Island, 2 Lippitt Rd., Kingston, RI, 02881, USA, Phone: (401)-874-2054, Fax: (401) 874-2380, E-mail: andreev@mail.uri.edu

Authors Contribution

MA, DW, OAA and YKR performed experimental work; MA, DME, OAA and YKR designed research; MA and YKR processed and analyzed data; MA and DW wrote the paper; DME, YKR and OAA edited the manuscript.

Manuscript Information: The number of characters including references, figure legends and figures is less than 39000 including spaces.

Abstract

We find that pHLIP-facilitated translocation of phalloidin, a cell-impermeable polar toxin, inhibited the proliferation of cancer cells in a pH-dependent fashion. The monomeric pH-(Low)-Insertion-Peptide (pHLIP) inserts its C-terminus across a membrane under slightly acidic conditions (pH 6-6.5), forming a transmembrane helix. The delivery construct carries phalloidin linked to its inserting C-terminus via a disulfide bond that is cleaved inside cells, releasing the toxin. To facilitate delivery of the polar agent, a lipophilic rhodamine moiety is also attached to the inserting end of pHLIP. After a 3h incubation at pH 6.1-6.2 with 2-4 μM concentrations of the construct, proliferation in cultures of HeLa, JC, and M4A4 cancer cells is severely disrupted (> 90% inhibition of cell growth observed). Treated cells also showed signs of cytoskeletal immobilization and multinucleation, consistent with the expected binding of phalloidin to F-actin, stabilizing the filaments against depolymerization. The antiproliferative effect was not observed without the hydrophobic facilitator (rhodamine). The biologically active delivery construct inserts into POPC lipid bilayers with an apparent pKa of ~ 6.15, similar to that of the parent pHLIP peptide. Sedimentation velocity experiments showed that the delivery construct is predominantly monomeric (> 90%) in solution under conditions employed to treat cells (pH 6.2, 4 μM). These results provide a lead for anti-tumor agents that would selectively destroy cells in acidic tumors. Such a targeted approach may both enhance the efficacy of cancer chemotherapy and reduce side effects.

Introduction

Cancer chemotherapy is often limited by the toxic side effects of anti-neoplastic agents. Targeted therapy, including targeted drug delivery, can improve the therapeutic index by reducing side effects in healthy tissues. Some drug delivery systems, such as liposomes and polymers, can passively target tumors due to the enhanced permeation and retention (EPR) effect (1-3). However, the EPR effect is small or nonexistent for certain tumors (2, 4-6). Most molecular targeting strategies take aim at specific cancer biomarker proteins such as over-expressed cell surface receptors. Antibodies and other molecules (e.g. transferrin, folate) have been used as targeting ligands to bind to these receptors for the delivery of therapeutic agents to cancer cells (7, 8). However, many cancer biomarker receptors (e.g. ERBB2) are not uniquely expressed in cancer cells but also in certain healthy cells, leading to side effects in patients (9). Further, therapy based on the targeting of specific binding sites is hampered by the heterogeneity of tumors, especially the differences among cells within a tumor (10, 11). The lack of homogeneously expressed target biomarkers (among cancer cells) and the ease with which cancer cells can circumvent a single (or a few) targeted protein(s) could explain why molecular targeting approaches (for direct therapy or drug delivery) have had limited success against solid tumors and are frequently associated with rapid development of resistance (9, 12). Therefore, it is important to ask whether other, more general features of cancer physiology might be exploited for targeted therapy against solid tumors.

Acidosis is a property of tumor microenvironments that may serve as a general biomarker (13-15), and we have developed an approach to target cells in tissues with a

low extracellular pH. Our strategy is based on the action of the pH (Low) Insertion Peptide (pHLIP) — a water-soluble peptide derived from the transmembrane (TM) helix C of bacteriorhodopsin (16). At pHs above 7, pHLIP in solution equilibrates to the surface of a lipid bilayer without inserting; At slightly acidic pH, pHLIP inserts with a pKa of ~ 6 *in vitro* to form a TM helix (16). At concentrations below 7 μM, pHLIP molecules predominantly exist as monomers in solution, and in the presence of lipid vesicles (lipid:pHLIP molar ratio > 250:1), the monomeric state is maintained throughout membrane association and insertion (17, 18). pHLIP does not cause membrane leakage in any of the membrane associated states (17, 19). In addition, pHLIP showed no toxicity to cells (at concentrations up to 10 μM at pH 6.5 for 1 h or 16 μM at pH 7.4 for 24 h) or animals (4 mg/kg in mice, followed for 2 months) (20, 21). The insertion process is unidirectional (C-terminus in), rapid (< 2 min in lipid vesicles) and reversible (upon pH increase to > 7) (17, 20, 22). The transition between the surface bound state and the inserted state is mediated by the protonation / deprotonation of Asp side-chains in the TM region (16, 21). These unique properties prompted us to test both (D)- and (L)-pHLIP as tumor-imaging vehicles in animals (mice and rats). When pHLIP is conjugated to a near-IR fluorescent dye (e.g. Cy5.5, AlexaFluor 750) or the positron emission tomography probe ^{64}Cu-DOTA, these pHLIP imaging constructs showed the ability to target acidic tissues in vivo, including tumors, kidneys, and sites of inflammation (21, 23). In mouse implant models, pHLIP-dye constructs found tumors, defined their borders with a high degree of accuracy (24), and accumulated in them, even when the tumor was very small (i.e., visually undetectable, ≤ 1 mm) (21).

Given its properties, it may be possible to use pHLIP for targeted intracellular delivery of therapeutic agents. Under acidic conditions, the folding of pHLIP across a membrane (into a TM helix) is exothermic (by ~ 2 kcal/mole) (18), and the insertion can move C-terminal cargo molecules across a lipid bilayer (20, 25). The cargo can be conjugated to the inserting C-terminus of pHLIP via an S-S disulfide bond that is cleaved inside cells, releasing cargo into the cytoplasm. Among cargos that have been successfully delivered to the cell cytoplasm in this fashion are: (a) fluorescent dyes (e.g. dansyl), (b) phalloidin-TRITC (1.3 kDa with LogP ≈ -0.05, where P is the octanol-water partition coefficient), (c) PNA (2.5 kDa), and (d) cyclic peptides (up to 850 Da with LogP ≈ -3) (20, 25). pHLIP-mediated intracellular delivery does not rely on receptor binding or endocytosis (20), rather, the cargo molecule is directly delivered across the plasma membrane. This pathway avoids the endosomal trapping of drug payloads — a noted deficiency for many drug delivery systems that rely on endocytosis for cellular entry (26). In short, as a targeted drug delivery vehicle, pHLIP possesses two key properties: (i) targeting of acidic tumors, and (ii) direct cytoplasmic delivery of therapeutic agents. Thus, we envision using pHLIP-mediated drug delivery to preferentially destroy tumor cells while sparing normal tissue. In this study, we quantitatively investigate the biological consequence of pHLIP-mediated phalloidin delivery to cancer cells, providing evidence of inhibition of cell proliferation.

Results

Phalloidin, a cytotoxin isolated from the Death Cap mushroom *Amanita phalloides*, binds tightly to actin filaments (K_d < 40 nM) and stabilizes them against depolymerization (27-29). Phalloidin is a polar, cell-impermeable, cyclic heptapeptide

(**Fig. 1**). When a sufficient amount of phalloidin is micro-injected into a cytoplasm, cell proliferation is inhibited (30). Previously, we demonstrated that phalloidin-TRITC (attached to the C-terminus of pHLIP) is translocated across the plasma membrane of HeLa, JC (breast adenocarcinoma) and TRAMP (prostate) cancer cells in a pH-dependent manner, inducing stabilization of actin cytoskeleton and formation of multinucleated cells (20). However, these results were obtained with a construct in which pHLIP-Cys is photo-crosslinked to phalloidin-TRITC (a phalloidin-rhodamine conjugate) via a thiol-reactive aryl azide linker (i.e. S-[2-(4-azidosalicyl-amido)ethylthiol]-2-thiopyridine). This synthetic approach was convenient for initial test experiments, but it is unsuitable for further studies because it results in an undefined mixture of products, partly due to the photo-crosslinking chemistry, and partly due to the fact that phalloidin-TRITC **4** is a mixture of stereo- and regio-isomers (see **Fig. 1** for its structural variations) (31). Here we present controlled studies using pure constructs.

Design and Syntheses of Delivery Constructs pHLIP-C(aminophalloidin) and pHLIP-K(rhodamine)-C(aminophalloidin)

To evaluate the therapeutic potential of phalloidin as a pHLIP-delivered cytotoxin, we need to use a chemically defined agent. Thus, we synthesized a single isomer pHLIP-C(aph) **5** in which amino-phalloidin (aph) is directly attached to the C-terminus Cys via a short disulfide linker (**Fig. 1**). The synthesis of pHLIP-C(aph) **5** begins with the commercially available single isomer amino-phalloidin **2**, which differs from phalloidin **1** only in that the terminal δ-hydroxyl group of side-chain 7 is replaced by an amino group (**Fig. 1**) (32). Treatment of amino-phalloidin **2** with the bifunctional

linker SPDP provided the pyridyl-disulfide-derivatized amino-phalloidin PDP intermediate **3** (**Fig. 1**), which was subsequently conjugated to pHLIP-Cys via disulfide exchange to give the final construct **5**. This two-step procedure was carried out without purification of intermediate **3**. To avoid side reactions and to simplify purification, near quantitative amounts of SPDP (1.2 eq.) and pHLIP-Cys (1.21 eq.) were added. HPLC purification provided the final construct **5** in > 90% purity and ~ 50% yield over two steps, and its identity was confirmed via MALDI-TOF MS. Among all phalloidin side-chains, the position-7 Leu-$(OH)_2$ side-chain is least important for binding to F-actin (31). Therefore, the short linker attaching amino-phalloidin to pHLIP-Cys in construct **5** is expected to have only a minimal effect on F-actin binding after release into the cytoplasm.

However, to our surprise, we could not find conditions under which the pHLIP-C(aph) construct stopped or suppressed growth in several cancer cell lines, including HeLa, JC, PC-3, and MCF-7 (see **Fig. 2e** for data with JC). Furthermore, pHLIP-C(aph) did not induce the expected cytotoxic effects, such as multi-nucleation or cytoskeleton rigidification, which were observed with the previous construct pHLIP-S-S-(phalloidin-TRITC) (20). Why does pHLIP translocate phalloidin-TRITC into cells more effectively than phalloidin alone? One explanation is that the hydrophobic rhodamine dye (i.e. TRITC) renders phalloidin-TRITC less polar than phalloidin, thus reducing the energetic barrier for translocation. Indeed, *n*-octanol/water partition experiments indicate that phalloidin-TRITC is extracted into the *n*-octanol phase ~ 40x more readily than phalloidin, with a LogP value of -0.05 compared to that of -1.5 for phalloidin (**Fig. 1**). If we consider the contribution of linker structures to cargo

polarity, the Log P difference between the two cargos could be even more pronounced, since the aryl azide photo-crosslinker used in pHLIP-S-S-(phalloidin-TRITC) is more hydrophobic than the SPDP-derived linker in pHLIP-C(aph). In short, we hypothesized that the hydrophobicity of the cargo correlates with the efficiency of pHLIP-mediated translocation, and in turn, the ability to induce biological effects in cells. To test this idea, we synthesized the pHLIP-K(rho)C(aph) construct **6,** in which a rhodamine (rho) moiety (i.e. TAMRA) is placed on a Lys residue immediately preceding the Cys residue carrying phalloidin (**Fig. 1**). We designed this construct so that the combined hydrophobicity of phalloidin and TAMRA should be similar to that of phalloidin-TRITC. The pHLIP-K-C(aph) intermediate (without the rho moiety) is synthesized and purified in the same fashion as described above for pHLIP-C(aph) **5**. By capping the amino terminus with an acetyl group (during solid-phase synthesis of the pHLIP-KC peptide), the rho moiety was then selectively conjugated to the Lys side-chain using the succimidyl ester of 5-TAMRA. This sequence provides the final construct pHLIP-K(rho)C(aph) **6** in ~ 27% overall yield in three steps.

Antiproliferative Effects of pHLIP-K(rhodamine)C(aminophalloidin)

When HeLa cells were treated with pHLIP-K(rho)C(aph) for 3 h at pH 6.2 (37ºC), cell proliferation was severely disrupted (**Fig. 2a**). Treatments were carried out at delivery construct concentrations ranging from 1 to 4 μM, in 96-well plates with ~ 4,000 cells per well. After 4 days of growth at normal pH, wells treated with 4 μM of pHLIP-K(rho)C(aph) contained almost no viable cells. Up to 97% inhibition of cell growth was achieved. Meanwhile, cells treated with only DMSO (0 μM column in **Fig. 2a**) had proliferated to ~ 60,000 cells per well. The anti-proliferative effect is

concentration dependent: when HeLa cells were treated at 1 and 2 μM concentrations, 31% and 71% inhibitions were observed, respectively. As expected, inhibition of cell growth is pH-dependent: treatment with pHLIP-K(rho)C(aph) at pH 7.4 under the same conditions had no effect on cell proliferation (**Fig. 2a**). This is consistent with the notion that delivery of phalloidin is mediated by pH-dependent pHLIP insertion across the plasma membrane, and does not involve endocytosis, which is expected to occur readily at pH 7.4. The low pH treatment in itself did not have any deleterious effect on the proliferation of HeLa cells, as shown by control experiments without pHLIP-K(rho)C(aph) (**Fig. 2a.** compare the 0 μM, pH 6.2, black bar with the 0 μM, pH 7.4, grey bar, there is no significant difference).

To check for cell-specific effects, we tested pHLIP-K(rho)C(aph) using JC (mouse mammary gland adenocarcinoma) and M4A4 (human breast ductal carcinoma) cells (**Fig. 2b/c**). In order to inhibit JC cell growth, the pH of the incubation media had to be further lowered to pH 6.1. The JC and M4A4 cells were more sensitive to low pH than HeLa cells, evidenced by non-specific cell death at pH 6.1-6.2 that reduced the number of viable cells by ~ 40-50% (**Fig. 2b/c**: 0 μM, black bar vs. grey bar). Nonetheless, growth inhibition specific to the presence of pHLIP-K(rho)C(aph) is evident: treatment with 2 μM of pHLIP-K(rho)C(aph) inhibited 78% of JC proliferation (**Fig. 2b**, pH 6.1 black bars: 2 μM vs. 0 μM), while 92% inhibition of M4A4 proliferation was observed at 4 μM (**Fig. 2c**, pH 6.2 black bars: 4 μM vs. 0 μM). Compared to the 0 μM controls at pH 6.2, reductions in the growth of JC and M4A4 cells are statistically highly significant (p-value < 0.001) even at 2 μM of

delivery construct. In short, the anti-proliferation effects observed with HeLa cells are reproducible with JC and M4A4 cells.

As expected, under equivalent conditions phalloidin (or aminophalloidin) showed no inhibitory effect on M4A4 / HeLa proliferation (**Fig. 2f**, data for phalloidin with M4A4 cells shown), consistent with the knowledge that phalloidin is a cell-impermeable toxin (30, 31). The rhodamine moiety on pHLIP-K(rho)C(aph) is necessary for inhibition, since: (a) under the same conditions pHLIP-C(aph) **5** does not stop the growth of JC or HeLa cells (**Fig. 2e**, data with JC cells shown); and (b) no inhibitory effect was observed when HeLa cells were treated with pHLIP-K-C(aph)—a construct missing the rhodamine moiety but otherwise identical to pHLIP-K(rho)C(aph) (**Fig. 2d**). However, in the case of pHLIP-K-C(aph), we cannot rule out the possibility that the positively charged free Lys side-chain in the C-terminus further burdens pHLIP insertion, blocking cargo entry. Furthermore, when HeLa cells were treated with an unmodified, 'native' pHLIP peptide that does not contain Lys or Cys in its C-terminus (thus with no rhodamine or phalloidin cargo attached), no inhibition of proliferation was observed (**Fig. S1**). Hence, pHLIP insertion in itself does not hinder cell growth, consistent with our previous observations that pHLIP is minimally toxic (20, 21). In summary, these data support our hypothesis that the combined hydrophobicity of the cargos, manifested as an overall property of the inserting C-terminus of pHLIP with its cargo, determines the efficiency of delivery into cells.

Morphological Changes of Cells Treated with pHLIP-K(rhodamine)C(aminophalloidin)

As observed previously (in cells incubated with the heterogeneous pHLIP-S-S-(phalloidin-TRITC) construct), HeLa cells treated with pHLIP-K(rho)C(aph) showed signs of cytoskeletal immobilization. After incubation with 4 μM of pHLIP-K(rho)C(aph) at pH 6.1 for 3 h, HeLa (**Fig. 3**) or M4A4 (**Fig. S2**) cells exhibited a reduced ability to contract and 'round up' when trypsinized, whereas cells treated at pH 7 detached and rounded as expected (**Fig. 3**). A subpopulation of the cells treated at low pH also became multinucleated (**Fig. 4**). Both observations are consistent with a view that pHLIP-K(rho)C(aph) delivers the toxic cargo across the plasma membrane, and that the released phalloidin binds to actin filaments to stabilize them, interfering with the F-actin turnover required both for cytokinesis and for cell contraction.

Discussion

We have studied the use of pHLIP to deliver cell-impermeable agents across membranes, anticipating that success might expand opportunities for the delivery of therapeutic molecules to treat cancer. We find that pHLIP-mediated translocation of phalloidin can inhibit the proliferation of cancer cells in a pH-dependent fashion. A single 3 h treatment with 4 μM of delivery construct pHLIP-K(rho)C(aph) at pH 6.1-6.2 led to more than 90% inhibition of HeLa and M4A4 cell growth, and the antiproliferative effect is absent at pH 7.4. Treated cells also showed signs of cytoskeletal immobilization and multinucleation, consistent with the expected binding of phalloidin to F-actin, stabilizing the filaments against depolymerization.

The level of inhibition of cell proliferation should be directly correlated with the amount of phalloidin translocated by pHLIP into cells. Actin is one of the most abundant proteins in eukaryotic cells, with a cytoplasmic concentration reaching 63

μM in fission yeast (or ~ 1.4 million monomers for a 92 μm^3 cell, counting both F- and G-actin) (33), and the local actin concentration can be as high as 460 μM in the division site (i.e. the mature contractile ring of fission yeast undergoing cytokinesis) (33) and 650 μM in lamellipodia of mouse melanoma cells (34). In this respect, targeting actin sets a stringent test for the delivery potential of pHLIP in general. How many copies of toxin can pHLIP deliver per cell? What maximum intracellular toxin concentration can pHLIP build up? And, more specifically, what critical intracellular concentration of phalloidin must have been delivered by pHLIP-K(rho)C(aph) in order to disrupt cell proliferation?

Although we do not know the exact amount of phalloidin delivered by our construct, it is possible to calibrate the levels of cell growth inhibition obtained with pHLIP-K(rho)C(aph) using the known antiproliferative effects of phalloidin. Weber and coworkers showed that in order to stop or delay the proliferation of PtK2 cells (rat kangaroo kidney epithelium), a micro-injection of a phalloidin stock solution of 1 or 0.2 mM is required, respectively, probably leading to a ~ 100 or 20 μM intracellular phalloidin concentration (30). Thus, by analogy, treatments with pHLIP-K(rho)C(aph) at 2-4 μM seem able to build-up cytoplasmic phalloidin concentration in the 20-100 μM range, matching the concentration of cytoplasmic actin. We estimate that this level of toxin build-up requires pHLIP to deliver 21 to 106 million phalloidin molecules per cell, calculated for HeLa cells in suspension with a 15-μm average diameter (1767 μm^3 volume) (**Fig. 3**), which in turn, implies that pHLIP-K(rho)C(ach) occupies 1.3 to 6.7 % of the plasma membrane area available for insertion in the attached cell (taking a pHLIP cross section area of ~ 113 $Å^2$ in the inserted state, and an available cell

surface area of 1800 μm^2, estimated from **Fig. 3**). Thus, perhaps a near-saturating level of inserted pHLIP-K(rho)C(aph) is needed to build up a 100 μM intracellular concentration of phalloidin in HeLa cells, which likely represents an upper limit of what is possible with pHLIP-mediated delivery.

In addition, we studied the insertion behavior of pHLIP-K(rho)C(aph) into liposomes (see SI text for details). By following changes in Trp fluorescence, we deduced that pHLIP-K(rho)C(aph) inserts into 1-palmitoyl-2-oleoyl-sn-glycero-3-phosphocholine (POPC) lipid bilayers with an apparent pKa of ~ 6.16 (**Fig. S3**). This value is similar to that of the parent pHLIP peptide (without any cargo) (16), and consistent with the level of acidity required for antiproliferative effects in cell experiments (i.e. pH 6.1-6.2). Further, sedimentation velocity experiments showed that pHLIP-K(rho)C(aph) is predominantly monomeric (> 90%) in solution under conditions employed to treat cells (i.e. pH 6.2, 4 μM, physiological ionic strength) (**Fig. S4**).

To facilitate phalloidin delivery, a lipophilic rhodamine moiety is also attached to the inserting end of pHLIP-K(rho)C(aph). An antiproliferative effect was not observed without the hydrophobic facilitator. Liposome studies showed that the failed construct pHLIP-C(aph) also seems able to insert into POPC membranes with a pKa of ~ 6.14 (see SI text and **Fig. S3**) and it is also predominantly monomeric (>80%) at 4 μM concentration, pH 6.2 (**Fig. S4**). However, we cannot exclude the possibility that during insertion pHLIP-C(aph) is trapped in a partially-inserted intermediate and no translocation of cargo occurs (see SI text for further discussion). It is also possible that there is a property (or a set of properties) that alters delivery efficiency in cells between these two constructs, but not in vesicles, resulting in an insufficient amount of

phalloidin delivered by pHLIP-C(aph). Possible factors include kinetic differences in the association with and/or insertion into the plasma membrane, influenced by parameters present only in the cells, such as the membrane potential, cholesterol content, membrane protein content, surface glycosylation, and other lipid compositional variables. Further work will be needed to explore such factors.

In summary, we showed that pHLIP-K(rho)C(aph) can deliver enough phalloidin molecules to kill cancer cells *in vitro* at pH 6.2 but has no effect on cells at neutral pH. This work opens new avenues of investigation to evolve anti-tumor agents that preferentially destroy cancer cells in acidic solid tumors, while minimally affecting cells in normal tissues, and to use therapeutic molecules that do not enter cells on their own.

Materials and Methods

A more detailed description of the anti-proliferative assays, as well as experimental procedures of the syntheses of pHLIP-C(aph) and pHLIP-K(rho)C(aph), cell culture, cell morphology assays and microscopy, liposome preparation, Trp fluorescence spectroscopy, analytical ultracentrifugation (sedimentation velocity experiments), Log P measurements and information about data analysis and the stability of delivery constructs are available on-line in the Supporting Information (SI).

Antiproliferation Assays. Stock solutions of pHLIP-C(aph) **5**, pHLIP-K(rho)C(aph) **6**, phalloidin **1**, pHLIP-K-C(aph) and pHLIP were prepared in DMSO at 200 μM concentration. HeLa, JC or M4A4 cells were seeded in 96-well plates (Costar) at a density of ~ 1,000 cell per well, and then grown for 2 days before treatment. DMSO stock of pHLIP-K(rho)C(aph) (or a control agent) was diluted with pH-adjusted,

sterile Leibovitz's L-15 Phenol Free Medium (L-15) to give treatment solutions in the 0.25 - 4 μM range. Appropriate amounts of DMSO were added to ensure that all treatment samples contain ~ 2% by volume. After removal of cell media, the L-15 treatment solution was added to each well (volume for HeLa plate: 80 μL per well; JC and M4A4: 160 μL), and then the plate was incubated at 37°C for 3 h. To minimize week-to-week cell variability, treatments at pH 6.1/6.2 and 7.4 were carried out on the same 96-well plate and all negative control data shown (in **Fig. 2d/e/f** and **S1**) are from plates in which positive results were also obtained. After treatment, 200 μL of normal media was added to each well before returning the plate to the incubator. Cell density of the '0 μM, pH 7.4' controls usually reached 40,000 to 80,000 cells per well after 3-6 days of growth. The viable cell number was quantified using the MTS reagent (Promega CellTiter 96 AQueous One Solution Cell Proliferation Assay). OD 490 nm values were obtained using a plate reader (Spectramax M2 from Molecular Devices).

Acknowledgements

The authors thank Dr. Lan Yao (Department of Physics, University of Rhode Island, Kingston) and Dr. William H. Brissette for their important experimental advice. We also thank Dr. Damien Thevenin and Dr. Francisco Barrera Olivares for discussions and comments on the manuscript. This work was supported by NIH grants GM073857 to DME and CA133890 to OAA, DME and YRK, and by an Anna Fuller Fund Postdoctoral Fellowship in Molecular Oncology to MA.

References

1. Matsumura Y & Maeda H (1986) A new concept for macromolecular therapeutics in cancer chemotherapy: mechanism of tumoritropic accumulation of proteins and the antitumor agent SMANCS. *Cancer Res* 46:6387-6392.

2. Maeda H, Bharate GY, & Daruwalla J (2009) Polymeric drugs for efficient tumor-targeted drug delivery based on EPR-effect. *Eur J Pharm Biopharm* 71(3):409-419.

3. Jain RK (1987) Transport of molecules in the tumor interstitium: a review. *Cancer Res* 47(12):3039-3051.

4. Sarapa N, *et al.* (2003) Assessment of normal and tumor tissue uptake of MAG-CPT, a polymer-bound prodrug of camptothecin, in patients undergoing elective surgery for colorectal carcinoma. *Cancer Chemother Pharmacol* 52(5):424-430.

5. Yuan F, *et al.* (1994) Vascular permeability and microcirculation of gliomas and mammary carcinomas transplanted in rat and mouse cranial windows. *Cancer Res* 54(17):4564-4568.

6. Allen TM & Cullis PR (2004) Drug delivery systems: Entering the mainstream. *Science* 303(5665):1818-1822.

7. Allen TM (2002) Ligand-targeted therapeutics in anticancer therapy. *Nat Rev Cancer* 2(10):750-763.

8. Davis ME, Chen ZG, & Shin DM (2008) Nanoparticle therapeutics: an emerging treatment modality for cancer. *Nat Rev Drug Discov* 7(9):771-782.

9. Hynes NE & Lane HA (2005) ERBB receptors and cancer: the complexity of targeted inhibitors. *Nat Rev Cancer* 5(5):341-354.

10. Fox EJ, Salk JJ, & Loeb LA (2009) Cancer genome sequencing--an interim analysis. *Cancer Res* 69(12):4948-4950.

11. Li C, *et al.* (2007) Identification of pancreatic cancer stem cells. *Cancer Res* 67(3):1030-1037.

12. Hambley TW & Hait WN (2009) Is anticancer drug development heading in the right direction? *Cancer Res* 69(4):1259-1262.

13. Cairns R, Papandreou I, & Denko N (2006) Overcoming physiologic barriers to cancer treatment by molecularly targeting the tumor microenvironment. *Mol Cancer Res* 4(2):61-70.

14. Penet MF, *et al.* (2009) Noninvasive multiparametric imaging of metastasis-permissive microenvironments in a human prostate cancer xenograft. *Cancer Res* 69(22):8822-8829.

15. Gerweck LE & Seetharaman K (1996) Cellular pH gradient in tumor versus normal tissue: potential exploitation for the treatment of cancer. *Cancer Res* 56(6):1194-1198.

16. Hunt JF, Rath P, Rothschild KJ, & Engelman DM (1997) Spontaneous, pH-dependent membrane insertion of a transbilayer alpha-helix. *Biochemistry* 36(49):15177-15192.

17. Reshetnyak YK, Segala M, Andreev OA, & Engelman DM (2007) A monomeric membrane peptide that lives in three worlds: in solution, attached to, and inserted across lipid bilayers. *Biophys J* 93(7):2363-2372.

18. Reshetnyak YK, Andreev OA, Segala M, Markin VS, & Engelman DM (2008) Energetics of peptide (pHLIP) binding to and folding across a lipid bilayer membrane. *Proc Natl Acad Sci U S A* 105(40):15340-15345.

19. Zoonens M, Reshetnyak YK, & Engelman DM (2008) Bilayer interactions of pHLIP, a peptide that can deliver drugs and target tumors. *Biophys J* 95(1):225-235.

20. Reshetnyak YK, Andreev OA, Lehnert U, & Engelman DM (2006) Translocation of molecules into cells by pH-dependent insertion of a transmembrane helix. *Proc Natl Acad Sci U S A* 103(17):6460-6465.

21. Andreev OA, *et al.* (2007) Mechanism and uses of a membrane peptide that targets tumors and other acidic tissues in vivo. *Proc Natl Acad Sci U S A* 104(19):7893-7898.

22. Andreev OA, *et al.* (2010) pH (low) insertion peptide (pHLIP) inserts across a lipid bilayer as a helix and exits by a different path. *Proc Natl Acad Sci U S A* 107(9):4081-4086.

23. Vavere AL, *et al.* (2009) A novel technology for the imaging of acidic prostate tumors by positron emission tomography. *Cancer Res* 69(10):4510-4516.

24. Segala J, Engelman DM, Reshetnyak YK, & Andreev OA (2009) Accurate Analysis of Tumor Margins Using a Fluorescent pH Low Insertion Peptide (pHLIP). *Int J Mol Sci* 10(8):3478-3487.

25. Thevenin D, An M, & Engelman DM (2009) pHLIP-mediated translocation of membrane-impermeable molecules into cells. *Chem Biol* 16(7):754-762.

26. Torchilin VP (2006) Recent approaches to intracellular delivery of drugs and DNA and organelle targeting. *Annu Rev Biomed Eng* 8:343-375.

27. Wieland T (1977) Modification of actins by phallotoxins. *Naturwissenschaften* 64(6):303-309.

28. Faulstich H, Schafer AJ, & Weckauf M (1977) The dissociation of the phalloidin-actin complex. *Hoppe Seylers Z Physiol Chem* 358(2):181-184.

29. De La Cruz EM & Pollard TD (1994) Transient kinetic analysis of rhodamine phalloidin binding to actin filaments. *Biochemistry* 33(48):14387-14392.

30. Wehland J, Osborn M, & Weber K (1977) Phalloidin-induced actin polymerization in the cytoplasm of cultured cells interferes with cell locomotion and growth. *Proc Natl Acad Sci U S A* 74(12):5613-5617.

31. Wulf E, Deboben A, Bautz FA, Faulstich H, & Wieland T (1979) Fluorescent phallotoxin, a tool for the visualization of cellular actin. *Proc Natl Acad Sci U S A* 76(9):4498-4502.

32. Wieland T, Hollosi M, & Nassal M (1983) Components of the green deathcap mushroom (Amanita phalloides), LXI: delta-Aminophalloin, a 7-analogue of phalloidin, and some biochemically useful, including fluorescent derivatives. *Liebigs Ann Chem* 1983(9):1533-1540.

33. Wu JQ & Pollard TD (2005) Counting cytokinesis proteins globally and locally in fission yeast. *Science* 310(5746):310-314.

34. Koestler SA, *et al.* (2009) F- and G-actin concentrations in lamellipodia of moving cells. *PLoS One* 4(3):e4810.

35. Hack V, *et al.* (1998) The redox state as a correlate of senescence and wasting and as a target for therapeutic intervention. *Blood* 92(1):59-67.

36. Rompel A, *et al.* (1998) Sulfur K-edge x-ray absorption spectroscopy: a spectroscopic tool to examine the redox state of S-containing metabolites in vivo. *Proc Natl Acad Sci U S A* 95(11):6122-6127.

37. Schuck P (2000) Size-distribution analysis of macromolecules by sedimentation velocity ultracentrifugation and Lamm equation modeling. *Biophys J* 78(3):1606-1619.

Figures

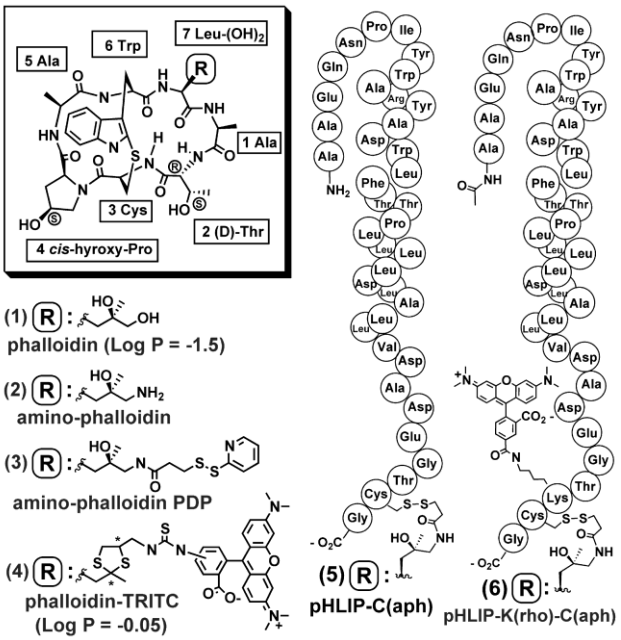

Figure 1. Structures of phalloidin and its derivatives are shown as **1** - **4**. For phalloidin-TRITC **4**, a star (∗) denotes a carbon center of mixed or unspecific stereochemistry. Structures of pHLIP delivery constructs tested in this study are shown as **5** and **6**.

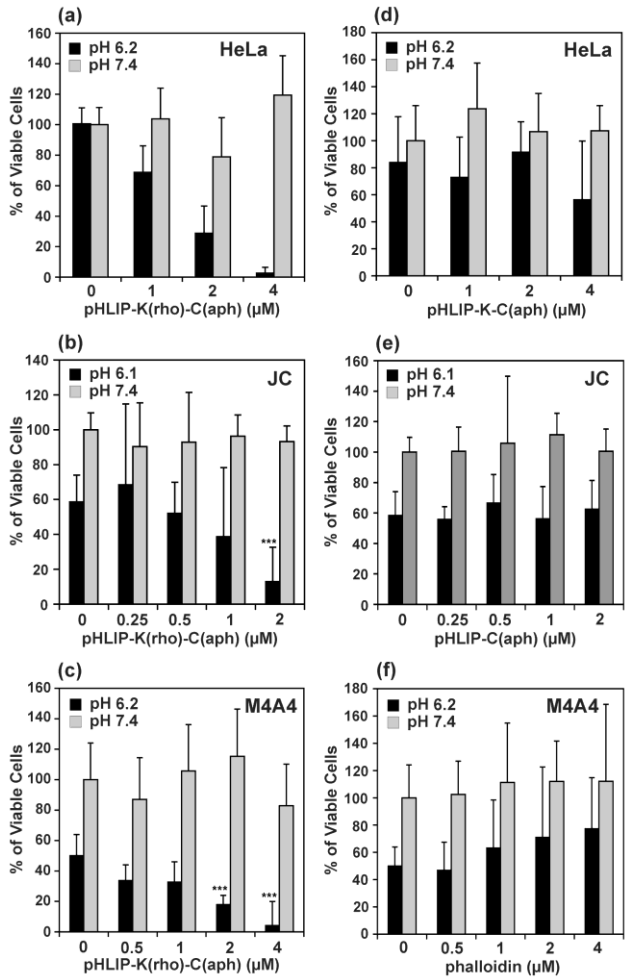

Figure 2. (a) Phalloidin delivery construct pHLIP-K(rho)C(aph) inhibits the proliferation of HeLa cells in a pH-dependent fashion. HeLa cells in 96-well plates (~ 4,000 cells per well) were incubated with 1, 2, or 4 μM of pHLIP-K(rho)C(aph) for 3 h at pH 6.2 (black bars) or 7.4 (grey). After 4 days of growth, the number of cells was estimated using the MTS tetrazolium reagent (with OD 490 nm as read-out). All OD 490 nm readings are normalized to the DMSO control (0 μM, pH 7.4) as 100%, which is ~ 60,000 to 70,000 cells per well. Errors of the means were estimated at the 95% confidence level using the two-tailed Student's T distribution coefficient (n = 12 except n = 4 for 4 μM at pH 7.4, see Supporting Information for more details). **(b)** Inhibition of proliferation of JC cells by pHLIP-K(rho)-C(aph) at pH 6.1 (n = 4 except

n = 8 for 0 μM data). A two-tailed Student's T-test with unequal variance (heteroscedastic) was carried out for the comparison of 0 μM and 2 μM pH 6.1 data sets (***: p-value = 0.00071). **(c)** Inhibition of proliferation of M4A4 cells by pHLIP-K(rho)-C(aph) at pH 6.2 (n = 4 except n = 8 for 0 μM data)**.** Two pairs of pH 6.2 data sets were compared: 0 μM vs. 2 μM (***: p-value = 0.00063) and 0 μM vs. 4 μM (***: p-value = 0.00015). **(d)** HeLa cells were treated with pHLIP-K-C(aph) (n = 4), and anti-proliferative effect was not observed. **(e)** pHLIP-C(aph) does not inhibit the proliferation of JC cells (n = 4 except n = 8 for 0 μM). **(f)** Phalloidin alone does not inhibit the proliferation of M4A4 cells (n = 4 except n = 8 for 0 μM).

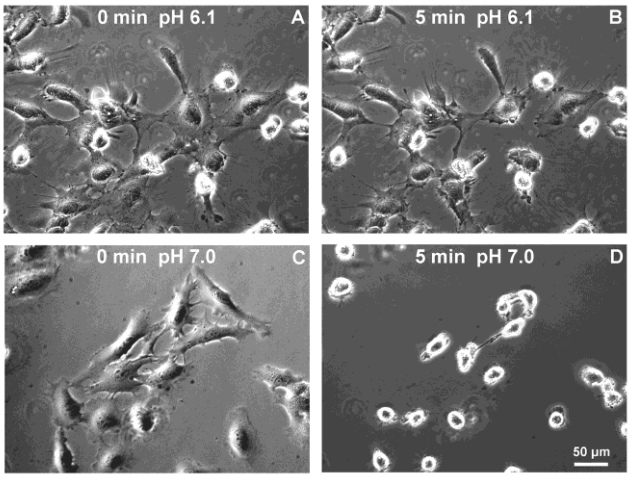

Figure 3. (A-D) Following incubation with pHLIP-K(rho)C(aph) (4 µM, 3 h) at pH 7, HeLa cells rounded and dissociated quickly after trypsinization: compare phase contrast image **C** taken before trypsinization with image **D** of the same view taken 5 min after addition of trypsin/EDTA. In contrast, HeLa cells treated with pHLIP-K(rho)C(aph) at pH 6.1 (also 4 µM, 3 h) could not easily contract—a sign of cytoskeleton rigidification, evident from images taken before **(A)** and 5 min after **(B)** the addition of trypsin/EDTA solution.

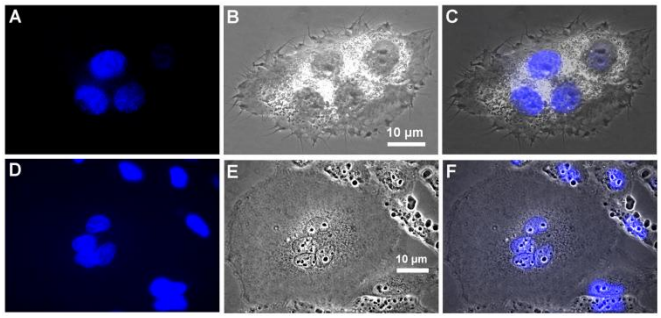

Figure 4. HeLa and M4A4 cells were treated with pHLIP-K(rho)C(aph) at 4 µM, pH 6.2 for 3 h. After 2-3 days of growth, a subpopulation of the treated cells became multinucleated. **(A)** 4',6-diamidino-2-phenylindole (DAPI) fluorescence image (artificial blue color) of a M4A4 cell with four nuclei (DAPI binds strongly to dsDNA and selectively stains the nucleus); **(B)** Phase contrast image of the same multinucleated M4A4 cell; **(C)** Overlay of images **A** and **B**; **(D)** DAPI fluorescence image of a HeLa cell with four nuclei; **(E)** Phase contrast image of the same HeLa cell, showing an unusually large volume of cytoplasm; **(F)** Overlay of **D** and **E**. These images were taken using an epi-fluorescence inverted microscope (Olympus IX71) with a 100x objective lens.

Supporting Information

Text

Determination of pKa of Insertion for pHLIP-K(rho)C(aph) and pHLIP-C(aph) by Following Changes in Trp Fluorescence

The insertion behavior of the delivery constructs was studied in 1-palmitoyl-2-oleoyl-sn-glycero-3-phosphocholine (POPC) model membranes using Trp fluorescence (excitation: 295 nm). Vesicles of POPC were prepared by extrusion (see below). The pHLIP sequence contains two Trp residues, both located in the transmembrane region. Upon helix formation and insertion, one Trp residue is likely positioned at the lipid headgroup region, while the other is in the hydrophobic interior of the bilayer (17). In addition, the phalloidin cargo has a modified Trp residue (whose side-chain is a part of the thio-ether transannular bridge, see **Fig. 1**); the maximum position of its absorbance spectrum is shifted to longer wavelengths ~ 290 nm (compared to 280 nm for Trp residues in pHLIP).

The emission maximum of pHLIP-C(aph) is centered on 350 nm at pH 8 (**Fig. S3a**). Lowering the pH leads to progressive emission maximum blue-shifts to ~ 338 nm, accompanied by increases in fluorescence intensity, and the blue-shift and intensity change are most pronounced between pH 6.2 and pH 5.9. These spectral changes are very similar to those observed for pHLIP alone (17), consistent with the transition of Trp residues from the lipid/water interface to more buried positions in the lipid bilayer.

A similar trend of spectral blue-shift is observed for pHLIP-K(rho)C(aph): when the pH is decreased from 7.9 to 5.2, the emission wavelength maximum shifts from ~ 346

nm to ~ 336 nm (**Fig. S3b**). However, the fluorescence intensity seems to peak between pH 6 and pH 5.5, and a further blue-shift of the emission maximum is accompanied by a decrease in fluorescence intensity (e.g. compare pH 5.7 yellow trace to pH 5.2 green trace in **Fig. S3b**). Perhaps this is due to more efficient quenching (both FRET and collisional quenching) of Trp fluorescence by the rhodamine moiety at lower pH, either intramolecularly, due to some inherent rhodamine pH-sensitivity, and/or intermolecularly (in the two-dimensional space of the membrane), in response to pHLIP insertion.

The apparent pKa of insertion is estimated from the progression of Trp emission maximum blue-shifts: for pHLIP-C(aph), the pKa value is 6.14 ± 0.02 (**Fig. S3c**), and for pHLIP-K(rho)C(aph) it is 6.16 ± 0.05 (**Fig. S3d**). Both agree very well with the previously reported pKa of insertion, ~ 6 for pHLIP (16). Taken together, these data support the notion that both pHLIP-K(rho)C(aph) and pHLIP-C(aph) insert into POPC bilayers in a pH-dependent fashion that is similar to pHLIP without any cargo.

However, in a strict sense, we do not know from these Trp fluorescence studies whether the phalloidin cargo is translocated all the way across the bilayer or not. Our kinetics studies indicate that more than 50% of changes in Trp fluorescence signals (both emission maximum blue-shifts and fluorescence intensity increase) are associated with pHLIP transition from the surface-bound unstructured state to the membrane-inserted helical intermediate(s) in which the helix is oriented parallel to the membrane surface (22). In the case of pHLIP-C(aph), it is possible that partially-inserted surface intermediate(s) might be trapped during insertion, thus the phalloidin

cargo remains in the extracellular space. Further investigation is needed to clarify this issue.

Materials and Methods (additional details)

pHLIP Peptides. The pHLIP, pHLIP-C and pHLIP-KC peptides were prepared by standard solid phase synthesis at the W.M. Keck Foundation Biotechnology Resources Laboratory (Yale University). Their sequences are listed below, with the approximate TM region denoted in italic and the C-terminal Cys and Lys residues in bold. In pHLIP-KC, the N-terminus NH_2 is capped with an acetyl group:

pHLIP:

NH_2-GGEQNP*IYWARYADWLFTTPLLLLDLALLV*DADEGT-CO_2H

pHLIP-C:

NH_2-AAEQNP*IYWARYADWLFTTPLLLLDLALLV*DADEGT**C**G-CO_2H.

pHLIP-KC:

Acetyl-NH-AAEQNP*IYWARYADWLFTTPLLLLDLALLV*DADEGT**KC**G-CO_2H.

Syntheses of pHLIP Conjugates. Aminophalloidin **2** (HCl salt) was purchased from Alexis Biochemicals (Enzo Life Sciences), *N*-succinimidyl 3-(2-pyridyl-dithio)-propionate (SPDP) from Sigma, and 5-carboxytetramethyl-rhodamine, succinimidyl ester (5-TAMRA, SE) from Invitrogen or Anaspec.

Synthesis of pHLIP-C(aph) 5. To a solution of amino-phalloidin **2** (1 mg, 1.21 µmole, 1 eq.) in 500 µL of aqueous (aq.) potassium phosphate buffer (100 mM, pH 7.5) was added a solution of SPDP (0.452 mg, 1.45 µmole, 1.2 eq.) in 226 µL of N,N-dimethylformamide (DMF). The reaction mixture was stirred at room temperature (r.t.) for 1.5 h. The progress of the reaction was monitored by reverse phase HPLC

(Hewlett Packard Zorbax semi-prep 9.4 x 250 mm SB-C18 column; flow rate: 2 mL/min; phase A: water + 0.01% TFA; phase B: acetonitrile + 0.01% TFA; gradient: 70 min from 99:1 A/B to 1:99 A/B): The starting material (s.m.) **2** elutes at 65:35 A/B, the SPDP linker elutes at 43:57 A/B, and the desired amino-phalloidin-PDP **3** product elutes at 52:48 A/B. This initial reaction is usually complete within 1 h. Afterwards, a solution of pHLIP-C (6.2 mg, 1.46 µmole, 1.21 eq., > 95% monomer) in 400 µL of argon-saturated DMF was added. The resulting mixture was stirred at r.t. under argon for 2.5 h. The desired final product pHLIP-C(aph) **5** was isolated via HPLC (**5** eluting at 35:65 A/B) in ~ 47% yield (0.57 µmole) over two steps, quantified using UV absorption at two wavelengths (ε_{280}=24,940 $M^{-1}cm^{-1}$, ε_{300}=14,000 $M^{-1}cm^{-1}$; all UV-vis absorbance spectra were obtained in aq. solutions of 6M guanidinium chloride). MALDI-TOF MS+ was used to confirm product identity: The molecular weight (MW) calculated for pHLIP-C(aph) **5** ($C_{234}H_{344}N_{54}O_{69}S_3$) is 5113.8, and the measured value was 5114.6, matching the predicted (MW + 1) value for MH+ (molecule plus proton) of 5114.8.

Synthesis of pHLIP-K(rho)-C(aph) 6.

Linker-derivatized amino-phalloidin-PDP **3** was synthesized as described above. Subsequently, a solution of pHLIP-KC (7.1 mg, 1.61 µmole, 1.33 eq.) in 1.6 mL of 1:1 DMF / aq. sodium phosphate buffer (100 mM, pH 8.0) was added, and the reaction mixture was stirred at r.t. under argon for 3 h. The progress of the disulfide-forming reaction was monitored using HPLC (s.m. pHLIP-KC eluting at 31:69 A/B, intermediate product pHLIP-K-C(aph) at 33:67 A/B; see above for HPLC methods). The intermediate pHLIP-K-C(aph) was isolated via HPLC in ~ 47% yield (0.56

μmole) over two steps, and quantified using UV absorption (ε_{280}=24,940 $M^{-1}cm^{-1}$, ε_{300}=14,000 $M^{-1}cm^{-1}$). MALDI-TOF MS+ gave an observed (MW + 1) value of 5285.7 (for MH+), compared with a calculated MW of 5284.0 for pHLIP-K-C(aph) ($C_{242}H_{358}N_{56}O_{71}S_3$).

For rhodamine conjugation, a solution of pHLIP-K-C(aph) (2.1 mg, 0.4 μmole, 1 eq.) in 770 μL of 2:3 acetonitrile / aq. sodium phosphate buffer (30 mM) was combined with a solution of 5-TAMRA-SE (0.76 mg, 1.44 μmole, 3.6 eq.) in 200 μL of 1:1 acetonitrile / water (final reaction pH: 8.0), and stirred at r.t. under argon in the dark for 12 h. The final product pHLIP-K(rho)-C(aph) **6** was isolated via HPLC (eluting at 30:70 A/B) in ~ 50% yield (0.2 μmole), quantified using UV-vis absorption at three wavelengths (ε_{560}=85,000 $M^{-1}cm^{-1}$, ε_{300}=27,603 $M^{-1}cm^{-1}$, ε_{280}=40,300 $M^{-1}cm^{-1}$). Some amount of the starting material pHLIP-K-C(aph) (up to 30%) was also collected and recycled. MALDI-TOF MS+ gave an observed (MW + 1) value of 5700.6 (for MH+), compared with a calculated MW of 5696.4 for pHLIP-K(rho)-C(aph) **6** ($C_{267}H_{378}N_{58}O_{75}S_3$).

Cell Cultures. Cancer cell lines (HeLa, JC, M4A4 and HT1080) were obtained from the American Type Culture Collection (ATCC): HeLa (CCL-2) is a human cervix adenocarcinoma cell line; JC (CRL-2116) is a mouse mammary gland adenocarcinoma cell line; M4A4 (CRL-2914) is a human breast ductal carcinoma cell line; and HT1080 (CCL-121) is a human connective tissue fibrosarcoma cell line. HeLa and M4A4 cells were cultured in DMEM ([+] 4.5 g/L D-glucose, [+] 40 mg/L sodium pyruvate, Gibco 10313), whereas JC cells were cultured in ATCC-formulated RPMI-1640 medium (with HEPES, sodium pyruvate, and L-glutamine, Cat No. 30-

2001), and HT1080 cells in ATCC-formulated Eagle's Minimum Essential Medium (Cat No. 30-2003). All cell growth media were supplemented with 10% FBS (Gibco) and ciprofloxacin-HCl (1 μg/mL) (from Cellgro, Voigt Global Distribution). Unless specified otherwise, cells were grown in an incubator (Revco Elite II, from Thermo Fisher Scientific) under a humidified atmosphere of air and 5% CO_2 at 37ºC.

Anti-Proliferation Assays. Stock solutions of pHLIP-C(aph) **5**, pHLIP-K(rho)C(aph) **6**, phalloidin **1**, amino-phalloidin **2**, pHLIP-K-C(aph) and pHLIP were prepared in DMSO at a concentration of 200 μM (**1** or **2**: ε_{280}=11,000 $M^{-1}cm^{-1}$, ε_{300}=10,100 $M^{-1}cm^{-1}$; pHLIP: ε_{280}=13,940 $M^{-1}cm^{-1}$) and stored at -20ºC. HeLa, JC or M4A4 cells were seeded in 96-well plates (Costar) at a density of ~ 1,000 cells per well, and then grown for 2 days (~ 2 doublings) before treatment. Leibovitz's L-15 Phenol Free Medium (L-15) was shaken with air (and/or incubated at 37ºC) to ensure that its final free thiol (SH) content is < 15 μM (estimated using the Ellman test), pH-adjusted to 6.1-6.2 or 7.4, and then sterilized via filtration through a 0.2 μm filter. Subsequently, the DMSO stock solution of pHLIP-K(rho)C(aph) (or a control agent) was diluted with the prepared L-15 to give treatment solutions in the 0.25-4 μM concentration range (see **Fig. 2** and **S1** for specific concentrations). Appropriate amounts of DMSO were added to ensure that all treatment samples contain the same amount of DMSO (~ 2% by volume), including the '0 μM' blank prepared by mixing L-15 with DMSO. The treatment solutions were vortexed, and then small portions were removed to measure the reported pH values, obtained at 23ºC (the pH values are ~ 0.15-0.2 unit lower when measured at 37ºC). After removal of cell media, the L-15 treatment solution was added to each well (volume for HeLa plate: 80 μL per well; JC and

M4A4: 160 µL), and then the plate was incubated at 37°C for 3 h. Afterwards, treatment solutions were collected and their pH values re-measured at 23ºC: A small up-drift in pH was sometimes observed for the low pH samples (e.g. HeLa: pH 6.2 → pH 6.5, M4A4: pH 6.1 → pH 6.3), while a down-drift was seen for the neutral pH samples (e.g. HeLa: pH 7.4 → pH 7.1, M4A4: pH 7.4 → pH 6.9). To minimize the effects of week-to-week cell variability, treatments at pH 6.1/6.2 and 7.4 were carried out on the same 96-well plate (pH 6.1/6.2: columns 1-5; pH 7.4: columns 7-11) and all negative control data shown (in **Fig. 2d/e/f** and **S1**) are from plates in which positive results were also obtained (pHLIP-K(rho)C(aph): rolls A-D; negative control: rolls E-H). After treatment, 200 µL of normal medium was added to each well before returning the plate to the incubator. Cell density in the '0 µM, pH 7.4' control wells usually reached 40,000 to 80,000 cells per well after 3-6 days of growth (depending on the cell line, e.g. the doubling time is 12-16 h for JC but 25-30 h for M4A4). The viable cell number was quantified using the MTS reagent (Promega CellTiter 96 AQueous One Solution Cell Proliferation Assay, with the One-Solution containing the tetrazolium compound 3-(4,5-dimethylthiazol-2-yl)-5-(3-carboxymethoxyphenyl)-2-(4-sulfophenyl)-2H-tetrazolium inner salt (MTS) and the electron coupling reagent phenazine ethosulfate (PES)): For each well, cell medium was replaced with 100 µL of PBS plus 20 µL of MTS/PES One-Solution stock (also added to control wells with no cells). After 1-3 h of incubation, OD 490 nm values were obtained using a plate reader (Spectramax M2 from Molecular Devices). After correcting for background (using cell free controls), the OD 490 nm readings are usually less than 0.7, in the range where the viable cell number has a linear relationship with OD 490 nm. All

values shown (**Fig. 2** and **S1**) are normalized to the DMSO-only control (0 μM) at pH 7.4 as 100%.

Cell incubations with pHLIP constructs were carried out in Leibovitz's L-15 Phenol Free medium, which contains ~ 1 mM cysteine/cystine in its formulation. We performed Ellman tests on L-15 (at pH 6.2 and 7.4) and found free thiol (SH) concentrations in the range of 5-13 μM, approximating the amount of free thiol in human plasma (10-15 μM) (35, 36). We were concerned that this free thiol content could prematurely cleave the disulfide bond in our constructs, releasing phalloidin before pHLIP can insert into cell plasma membranes. Therefore, an incubation sample (after treating HT1080 cells with 4 μM pHLIP-K(rho)C(aph) at pH 6.2 for 3 h) was analyzed by HPLC, which showed that no detectable decomposition of pHLIP-K(rho)C(aph) occurred during the cell incubation period.

The HPLC test also confirmed that pHLIP-K(rho)C(aph) was present in a large excess of the amount required to saturate the surfaces of ~ 4,000 cells. This is consistent with our observation that similar anti-proliferative results were obtained using either 80 or 160 μL of incubation volume per well. In theory, with 80 μL of 4 μM construct, the amount of pHLIP-K(rho)C(aph) present is in 453-fold excess of the number of constructs needed to deliver 106 million phalloidin molecules per HeLa cell (to build up the inhibitory 100 μM cytoplasmic concentration) for 4000 cells. In other words, the observed concentration dependence of inhibition in **Fig. 2a-c** is not due to lack of material (at lower concentrations), but rather to a kinetic effect. Perhaps the speed with which pHLIP-K(rho)C(aph) can saturate the cell surface and/or the speed of insertion are important limiting factors in the cell experiments.

In all cases, after incubation with pHLIP-K(rho)C(aph), cells became rhodamine-fluorescent, indicating association of the delivery construct to the cell surface (in both peripheral and inserted states). Cells treated at pH 6.2 were more fluorescent than cells treated at pH 7.4.

Cell Morphology Assays and Microscopy. HeLa or M4A4 cells were seeded in the center of a 35-mm dish with a 14-mm glass-bottom window coated with poly-d-Lys or collagen (MatTek Corp). After 2 days of culture (6,000-8,000 cells per dish), cells were incubated with 4 μM pHLIP-K(rho)C(aph) in L-15 for 3 h at pH 6.1 or 7.4 (volume: 160 μL, see above 'Anti-Proliferation Assays' section for details of preparation of treatment solutions).

Cell Dissociation Assay. After treatment with pHLIP-K(rho)-C(aph), cells were grown in normal media for 1 day, washed with PBS, and then 100 μL of Trypsin (0.25%) / EDTA cell dissociation solution (Gibco) was added to cells in 100 μL of PBS. Phase contrast images were taken before and after the addition of the Trypsin/EDTA solution, using an inverted epi-fluorescence microscope (Olympus IX71) with a 20x objective (and the software Q-Capture).

Multinucleation. After pHLIP-K(rho)-C(aph) treatment, cells were grown in normal media for two days, washed with PBS, incubated with the nucleus/DNA-staining fluorescent dye DAPI (5 μM in PBS) for 15 min, and then washed with PBS again. Phase contrast and DAPI fluorescence (488 nm emission) images were used to detect multi-nucleated cells (which usually constituted ~ 10-20% of the total population), acquired with an inverted epi-fluorescence microscope (Olympus IX71) equipped with a 100x oil objective lens and using the software Q-Capture.

Analytical Ultracentrifugation. To investigate the aggregation tendency of delivery constructs in solution under cell treatment conditions, sedimentation velocity experiments were carried out at matching conditions of 4 μM construct, pH 6.2 or 7.4, 37ºC, and in aqueous buffers with approximately physiological ionic strength (10 mM sodium phosphate, 150 mM NaCl). Samples were centrifuged at 35,000 rpm in a Beckman Optima XL-I for at least 9 h. Sedimentation of different construct species was followed by absorption at 280 nm, and all data were processed using SEDFIT to obtain the continuous sedimentation coefficient distribution (37), with the following parameters of c(s) analysis: frictional ratio of 1.3, partial specific volume of 0.73, buffer density of 1.00099 for pH 6.2 (or 1.00141 for pH 7.4), buffer viscosity of 0.00704 for pH 6.2 (or 0.00705 for pH 7.4), and F-ratio of 0.683. All data were fitted without back diffusion, which gave the best rmsd (ranging from 0.0058 to 0.0061).

As shown in **Fig. S4a**, at pH 6.2, the main species (95%) of pHLIP-K(rho)C(aph) has a sedimentation coefficient of 1.4 S, corresponding to a particle size of 6.79 kD, which likely represents the monomer (M.W. 5696). Not surprisingly, under the same conditions at pH 7.4, pHLIP-K(rho)C(aph) is also predominantly monomeric (**Fig. S4b**: 1.3 S, 5.99 kD, 96%). Further, the failed construct pHLIP-C(aph) (M.W. 5114) also seems to be mostly monomeric at pH 6.2 (**Fig. S4c**: 1.19 S, 5.28 kD, 81%), although the proportion of larger species (6.55 S, 68.4 kD, 9%) increased for this construct.

To test whether these delivery constructs decompose during sedimentation velocity or cell experiments, ultracentrifugation samples were analyzed via HPLC before and

after the spin (**Fig. S5**). In all cases, after being at 37ºC for more than 24 hours, chemical decomposition is modest (5-20%).

Liposome Preparation. One hundred nm diameter liposomes were prepared via extrusion. A solution of 5 mg of 1-palmitoyl-2-oleoyl-sn-glycero-3-phosphocholine (POPC) (Avanti Polar Lipids) in 0.2 mL of chloroform was dried in a small round-bottom flask in vacuo (using a rotary evaporator) and/or under a stream of argon, and then held under house vacuum overnight. The dry film of lipid residue was re-hydrated with 0.5 mL of aqueous sodium phosphate buffer (pH 8.0, [Pi]: ~ 5 mM) for 30 min and vortexed vigorously to obtain a multi-lamellar vesicle suspension ('[POPC]': ~ '13mM'). This mixture was freeze-thawed at least 7 times using a dry-ice/ethanol bath (-70ºC). Final extrusions were performed using an Avanti Mini-Extruder: At least 15 passages through a polycarbonate membrane with 100 nm sized pores (Whatman 800309: Schleicher & Schuell, Nuclepore Track-Etch Membrane, 0.1 µm) were carried out to give the desired large unilamellar vesicles.

Trp Fluorescence Measurements. ***Sample Preparation.*** A lyophilized sample or a concentrated aqueous stock of pHLIP-C(aph) or pHLIP-K(rho)C(aph) was dissolved in or diluted with an aqueous sodium phosphate buffer to reach the following final concentrations: [delivery construct]: 15-40 µM; [Pi]: ~ 1-5 mM (final pH: 7-8). This dilute stock was stored at room temperature for 24 h (or at 0ºC for at least 3 days), allowing pHLIP species to reach the appropriate oligomer / monomer equilibrium (deaggregation), and then the pHLIP construct concentration was estimated using UV-vis absorption (see synthesis section for details). The stock of delivery construct was further diluted with water (Millipore), vortexed and then incubated with POPC

vesicles for at least 2 h at pH 7.5-8 (to allow pHLIP constructs to partition to the lipid surface), with a final pHLIP-construct to lipid ratio of 1:260 and a pHLIP-construct concentration of 4 μM. To trigger pHLIP insertion, the pH of this mixture was adjusted to the desired value (between 4 and 8) using small volumes of concentrated sodium phosphate buffer (100 mM) of various pH (final concentrations: [Pi] ~ 10-12 mM; [pHLIP-construct] ~ 3.6 μM). Samples were then equilibrated at the final pH for at least 30 min (at room temperature) before Trp fluorescence measurements were made.

Trp Fluorescence Spectroscopy. Trp residues were excited at 295 nm, and fluorescence emission spectra were collected from 310-400 nm. Measurements were obtained using a SLM-Aminco 8000C spectrofluorimeter (ISS, Champaign, IL) equipped with a thermo-bath (model RTE-111, Neslab). All measurements were performed at 25ºC at the delivery construct concentration of 3.6 μM. The widths of the excitation and emission slits were set to 4- and 8-nm, respectively. All spectra (e.g. as shown in **Fig. S3a/b**) were corrected for background signals using spectra obtained with blank liposome solutions at pH 8, 7, 6, and 5 (the nearest pH blank was used for spectral subtraction) and smoothed via averaging of 5 adjacent data points.

The apparent pKa values shown in **Fig. S3 c/d** were calculated by fitting the transition curve, obtained by plotting the changes of the position of maximum of fluorescence spectra versus pH, to the Henderson-Hasselbalch equation (using the nonlinear fitting option in the software Origin 7):

$$y = A_2 + \frac{A_1 - A_2}{1 + 10^{n(pKa - x)}}$$

where *x* is the pH, y is the emission spectrum maximum wavelength, *pKa* is the apparent pKa of insertion into a POPC bilayer with *n* as the Hill coefficient (which reflects the cooperativity of the transition), and A_1 and A_2 are the maxima of the fluorescence spectra of constructs in the membrane-bound (i.e. high pH) and inserted (i.e. low pH) states, respectively. The pKa values in **Fig. S3 c/d** are presented as mean± st.d.

Log P Measurements. A 5-, 20-, or 50-μM solution of phalloidin (or phalloidin-TRITC) in 500 μL of PBS (pH 7.4) was mixed with 500 μL of *n*-octanol. The mixture was vortexed for 5 min, allowed to settle at room temperature for 6 h, and allowed to stand for up to 2 days at 4˚C. Afterwards, the octanol and PBS layers were separated and their UV absorbance measured (at 300 nm for phalloidin or at 545 nm for phalloidin-TRITC). We assumed that the molar extinction coefficients in *n*-octanol and PBS buffer are the same, and the ratio of the OD readings was used directly to calculate the Log P (*n*-octanol/water) values. The final Log P value of phalloidin or phalloidin-TRITC given in **Fig. 1** is the average of the Log P values obtained at 5-, 20-, and 50-μM concentrations. The phalloidin-TRITC sample shows several peaks in its HPLC trace, indicating that it is a mixture of diastereomers plus additional impurities (which may affect the overall Log P).

Statistics (for data shown in Fig 2 and S1). All standard errors of the mean are estimated at the 95% confidence level using the two-tailed confidence coefficient $t_{CL,\nu}$ in the Student's t test distribution with ν degrees of freedom (ν = n-1), according to the following equation:

$$\text{estimate of true value} \approx \overline{X_n} \pm t_{CL,\nu} \frac{S_n}{\sqrt{n}}$$

where $\overline{X_n}$ is the mean, S_n is the sample standard deviation and n is the sample size. In our experiments, n varies from 4 to 12 ($t_{CL,\nu} = 3.18$ when $n = 4$ and $t_{CL,\nu} = 2.20$ when $n = 12$).

Supporting Information Figures

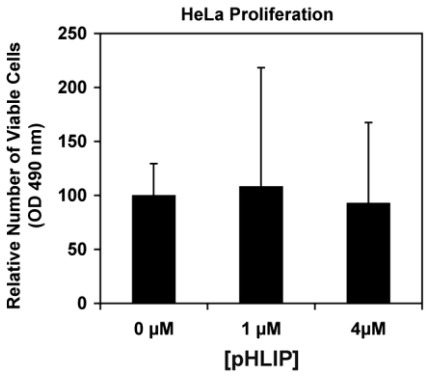

Figure S1. The parent pHLIP peptide (without cargo) does not inhibit cancer cell proliferation, confirming that pHLIP insertion in itself is benign to cells**.** HeLa cells were treated with pHLIP at pH ~ 6.2 as described for pHLIP-K(rho)-C(aph) experiments (n = 4).

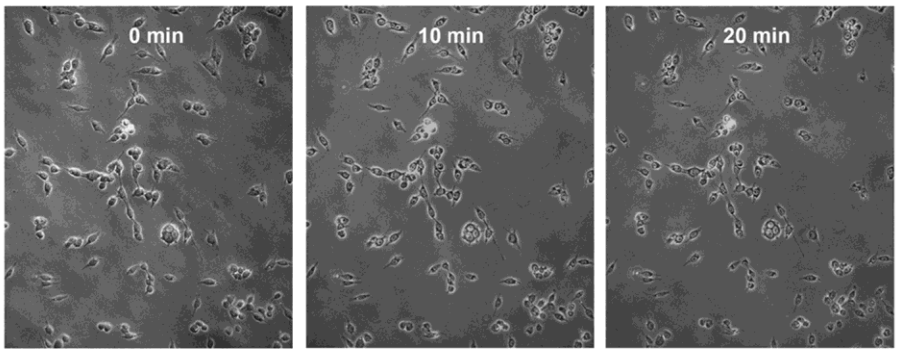

Figure S2. As with HeLa cells (**Fig 3**), M4A4 cells did not round-up when trypsinized after treatment with pHLIP-K(rho)C(aph) at pH 6.1-6.2. All trypsinizations were carried out at room temperature in PBS (at pH 7.4). The images were taken using an epi-fluorescence inverted microscope (Olympus IX71) with a 10x objective lens.

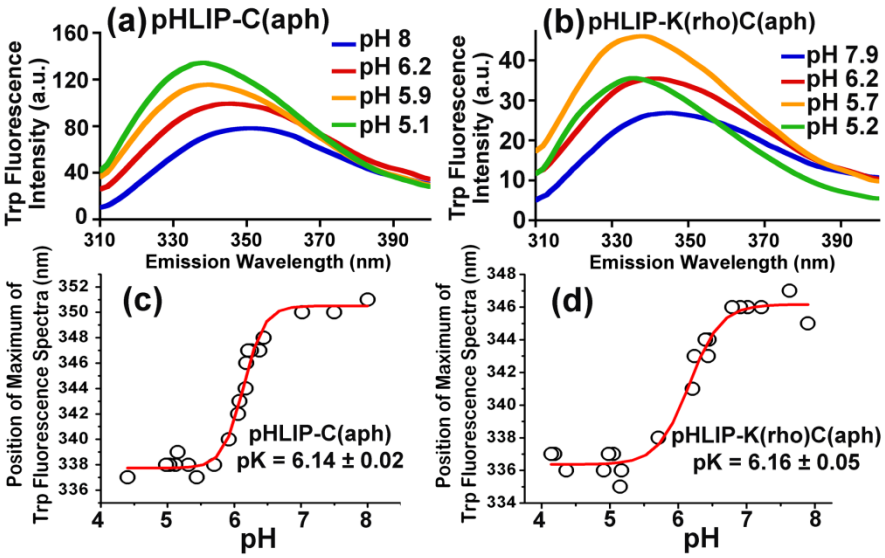

Figure S3. Trp fluorescence spectra of pHLIP-C(aph) **(a)** and pHLIP-K(rho)C(aph) **(b)** at different pH values in the presence of liposomes are shown. Apparent pKa values of insertion of pHLIP-C(aph) **(c)** and pHLIP-K(rho)C(aph) **(d)** into a POPC bilayer were calculated from the pH-dependent change of Trp fluorescence maxima according to the Henderson-Hasselbalch equation (see SI text for details).

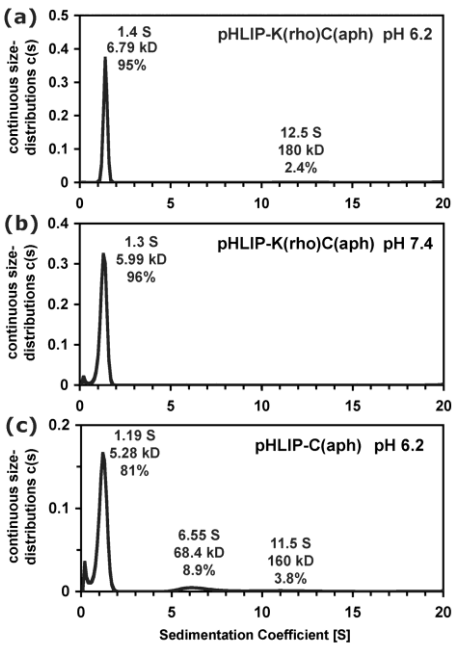

Figure S4. Sedimentation velocity experiments suggest that delivery constructs pHLIP-K(rho)C(aph) and pHLIP-C(aph) are predominantly monomeric under cell treatment conditions even at pH 6.2 (see SI text for details).

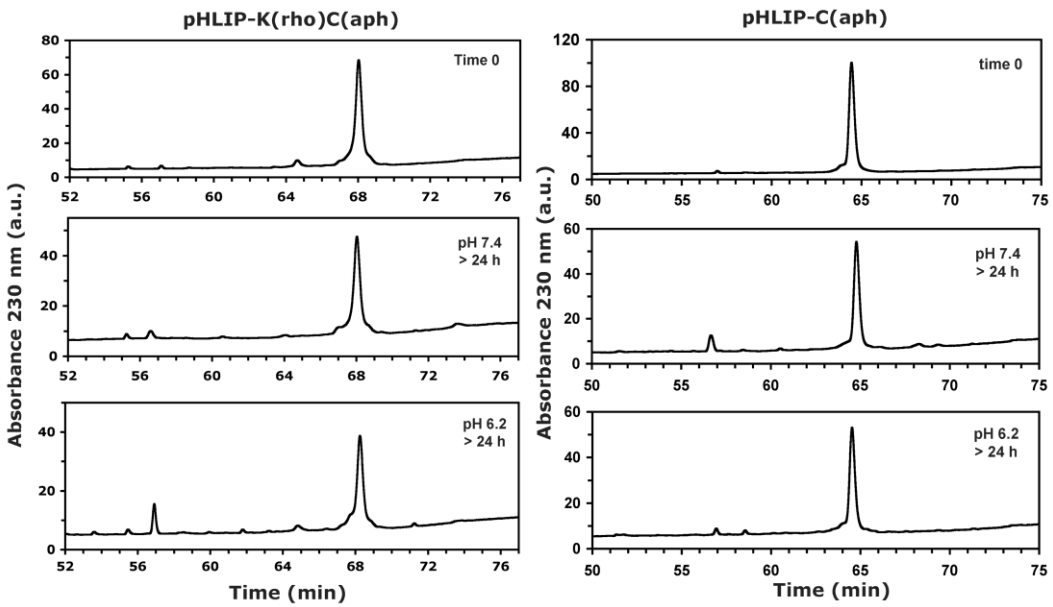

Figure S5. HPLC traces of pHLIP-K(rho)C(aph) and pHLIP-C(aph) samples (4 µM construct, at pH 6.2 or 7.4, with 10 mM sodium phosphate and 150 mM NaCl) before and after sedimentation velocity experiments show that these delivery constructs are chemically stable under conditions of analytical centrifugation and cell experiments. In all cases, only modest decomposition (< 20%) was observed after > 24 h at 37ºC.

CHAPTER 2

Submitted to Biochemistry journal

Tuning hydrophobicity of phallacidin cargo for improved translocation across plasma membrane by pH (Low) Insertion Peptide

Dayanjali Wijesinghe[1], Donald M. Engelman[2], Oleg A. Andreev[1], Yana K. Reshetnyak[1]

[1]Physics Department, University of Rhode Island, 2 Lippitt Rd., Kingston, RI, 02881, USA

[2]Department of Molecular Biophysics and Biochemistry, Yale University, P.O. Box 208114, New Haven, CT 06520, USA

TITLE RUNNING HEAD: Tuning hydrophobicity of cargo translocated by pHLIP

Corresponding Authors:

Yana K. Reshetnyak, Physics Department, University of Rhode Island, 2 Lippitt Rd., Kingston, RI, 02881, USA, Phone: (401)-874-2060, Fax: (401) 874-2380, E-mail: reshetnyak@mail.uri.edu

ABSTRACT

Drug molecules are typically hydrophobic and small in order to traverse membranes to reach cytoplasmic targets, but we have discovered that more polar molecules can be delivered across using water-soluble, moderately hydrophobic membrane peptides in the pHLIP (pH Low Insertion Peptide) family. Delivery of polar cargo molecules could expand the chemical landscape for pharmacological agents that have useful activity but are too polar by normal drug criteria. The spontaneous insertion and folding of the pHLIP peptide across a lipid bilayer seeks a free energy minimum, and insertion is accompanied by a release of energy that can be used to translocate cell-impermeable cargo molecules. In this study we report our first attempt to tune the hydrophobicity of a polar cargo, phallacidin, in a systematic manner. We present the design, synthesis and characterization of three phallacidin cargoes, where the hydrophobicity of the cargo was tuned by the attachment of diamines with various lengths of hydrophobic chains. The phallacidin cargo with a similar polarity to phallodin-rhodamine was conjugated to pHLIP, and shown to selectively inhibit the proliferation of cancer cells at low pH.

KEYWORDS: pHLIP, phallacidin, hydrophobicity, translocation across membrane, drug design, drug delivery, acidity

INTRODUCTION

Targeted drug delivery would allow drugs to preferentially affect diseased cells, enhancing therapeutic efficacy while reducing side effects. targeting could be particularly important for cancer therapy, since most anti-cancer drugs are toxic, not only killing cancer cells but also causing serious damage to healthy tissues. Despite significant progress toward drugs that specifically target protein biomarkers for certain kinds of cancer cells, there is still no "silver bullet" against cancer. One reason for the limited success so far is that cells in tumors are heterogeneous and selection for resistance to protein-targeted drugs and to the immune system can occur (1). An alternative might be to find a targeting mechanism that does not depend on a selectable marker. One of the universal differences between cancerous and normal tissues is that the former exhibit a significantly acidic extracellular environment. Acidosis is a hallmark of solid tumor development at both very early and advanced stages, as a consequence of anaerobic metabolism (the Pasteur effect) (2) and "aerobic glycolysis" known as the Warburg effect (3).

To target acidic tissues, we have developed a new approach, based on the action of a water-soluble, moderately hydrophobic membrane polypeptide, pHLIP (pH Low Insertion Peptide), derived from the bacteriorhodopsin C helix. pHLIP is a soluble peptide that was found to fold and insert across a membrane to form a stable transmembrane alpha helix under acidic conditions (4). When triggered by low pH,

members of the pHLIP peptide family act as monomeric, membrane-inserting peptides that translocate their carboxyl termini across membranes into the cytoplasms of targeted cells, while the amino termini remain in the extracellular space, locating the peptide across the plasma membrane lipid bilayers (5). Because the insertion occurs at low pH, acidic tissues are targeted, and so pHLIP has a dual delivery capability: it can tether N-terminus linked cargo molecules to the surfaces of cells in diseased tissues and it can move a C-terminus linked, cell-impermeable cargo molecule across the membrane into the cytoplasm using the free energy of insertion (6, 7). Use of a cleavable link, such as a disulfide, releases the cargo inside the cell (8, 9). Low pH leads to the protonation of negatively charged residues (Asp or Glu), which enhances peptide hydrophobicity, increasing the affinity of the peptide for the lipid bilayer and triggering peptide folding and subsequent membrane insertion (10, 11). The source of energy for moving polar molecules attached to pHLIP through the hydrophobic layer of a membrane is the membrane-associated folding of the polypeptide (12, 13). The affinity of peptide for a membrane at low pH is about 5 times higher than at high pH, allowing pHLIP to distinguish and mark acidic diseased tissue (10, 14, 15) associated with various pathological states, such as cancerous tumors, inflammation, ischemia, stroke and others.

Our recent findings indicate that pHLIP facilitates the translocation of phalloidin, a cell-impermeable polar toxin, which leads to the inhibition of the proliferation of cancer cells in a pH-dependent fashion (8). However, the antiproliferative effect was observed only when a hydrophobic facilitator (rhodamine) was attached to the peptide

inserting end. An alternative approach is to modify the properties of the cargo molecule to optimize delivery, and the goal of this study is to tune properties of the pHLIP-cargo constructs to achieve the most efficient pH-dependent translocation of cargo molecules across the lipid bilayer. The properties of a molecule delivered into cells will help to define the chemical landscape available for the use of pHLIP. Here we present the design, synthesis and characterization of three phallacidin cargoes, where the hydrophobicity of the cargo was tuned by attachment of diamines having various lengths of hydrophobic chains. We have selected one of the phallacidin cargoes (phallC6SH) of similar polarity as phallodin-rhodamine, synthesized and characterized pHLIP-C6phall construct, and tested the antiproliferative effect on cultured cells.

MATERIALS AND METHODS

Peptide preparation

The pHLIP peptide (AEQNPIYWARYADWLFTTPLLLLDLALLVDADEGCT) was prepared by solid-phase peptide synthesis at the W.M. Keck Foundation Biotechnology Resource Laboratory at Yale University. The lyophilized powder was soluble in 3 M urea or DMSO (dimethyl sulfoxide). When dissolved in urea the peptide was transferred to buffer using a G-10 size-exclusion spin column. The concentration of the peptide was determined spectrophotometricly by measuring absorbance at 280 nm (ε_{280}=13,940 $M^{-1}cm^{-1}$).

Synthesis of phallacidin-$(CH_2)_n$-SH

Materials. Phallacidin was purchased from GenoLite Biotek, *N*-hydroxysuccinimide (NHS), *N, N'*-dicyclohexylcarbodiimide (DCC), *N*-succinimidyl 3-(2-pyridyl-dithio)-propionate (SPDP) were from Thermo Scientific, Hexamethylenediamine 98%, 1,4-diaminobutane 99%, 1,10-diaminodecane 97% were from Sigma Aldrich.

Step1: Phallacidin (2.6 mg, 3.10 µmol) was dissolved in 100 µl dry DMF (dimethylformamide) and transferred into a 1.5 ml glass vial followed by addition of NHS (2.5 mg, 21.6 µmol, 7 eq) in 30 µl dry DMF and mixed well. DCC (1.15 mg, 5.57 µmol, 1.8 eq) was added to the reaction mixture. The reaction mixture was stirred at room temperature overnight, then the reaction mixture was centrifuged and separated from the urea crystals. The progress of the reaction was monitored by reverse phase HPLC (high-performance liquid chromatography) at t=0 and at t=12 hrs. (Agilent Technologies Zorbax SB-C184.6 x 250 mm column; flow rate 1 ml/min; phase A water + 0.05% TFA (trifluoroacetic acid); phase B acetonitrile + 0.05% TFA; gradient 30 min from 95:5 A/B to 50:50 A/B) The phallacidin starting material elutes at 24.9 min, while activated hydroxysuccinimidephallacidin elutes at 23.6 min. The reaction is comple by 12 hrs.

Step2: The supernatant from the step 1, which contained the activated hydroxysuccinimidephallacidin was added into diamines $H_2N\text{-}(CH_2)_n\text{-}NH_2$ (n=4, 6 or 10) dissolved in dry DMF (31 µmol, 10 eq of phallacidin) and the reaction mixture was stirred at room temperature for 10 hrs. The addition of the diamine resulted in the formation of a precipitate: dehydrated phallacidin diamine salt. The product,

phallacidin-$(CH_2)_nNH_2$ (phallCn) was found both in the precipitate and in the supernatant. The precipitate was separated by centrifugation and dissolved in 120 µl MeOH/H_2O (1:1). The product was purified using HPLC and lyophilized. The elution times of phallacidin-$(CH_2)_4NH_2$ (phallC4), phallacidin-$(CH_2)_6NH_2$ (phallC6) and phallacidin-$(CH_2)_{10}NH_2$ (phallC10) were 23.1, 24.6 and 29.5 min, respectively as expected from the increasing hydrophobicities. The lyophilized powder was then dissolved in 100 µl of MeOH/H_2O (1:1), quantified by measuring OD (optical density) at 300 nm (ε_{300} of phallacidin: 10,100 $M^{-1}cm^{-1}$) and analyzed using ESI (electronspray ionization) mass spectrometry. Molecular weights (MW) of the phallotoxins phallC4, phallC6 and phallC10 were 917.23, 945.18 and 1001.22 Da, respectively (the expected MWs are 917.06, 945.12 and 1001.23 Da).

Step 3: The products from step 2 (in 100 µl of MeOH/Water 1:1) were transferred into 200 µl of 100 mM phosphate buffer at pH 8. A solution of SPDP (starting from 5 eq of phallCn) in DMSO was added to the reaction mixture and stirred at room temperature. After about 2 hrs, most of the SPDP was hydrolyzed to PDP and no further progression of formation of the phallCn-PDP was observed. The pH of the reaction mixture was adjusted to pH 8 and more SPDP was added until almost all phallCn was reacted. The progress of the reaction was monitored using HPLC. Phallacidin-$(CH_2)_n$-SH (phallCnSH) was obtained by reducing the disulfide bond in the phallCn-PDP using TCEP (20 eq to SPDP added) in 100 mM phosphate buffer pH 8 for 30 min, purified using reverse phase C18 HPLC, lyophilized, and characterized using ESI mass spectrometry. The elution times and MWs of phallotoxins on HPLC runs with 30

min gradients from 99:1 A/B to 70:30 A/B (flow rate 1 ml/min) were: for phallacidin 30.3 min/ 846.15 Da, for phallC_4SH 32.4 min/1005.17 Da, for phallC_6SH 35.5 min/1033.03 Da and for phallC_{10}SH 44.4 min/1089.07 Da.

Synthesis of pHLIP-S-S-$(CH_2)_6$-phallacidin (pHLIP-C6phall). phallC6-PDP was synthesized as described above, purified using HPLC, and lyophilized. The lyophilized phallC6-PDP was dissolved in DMSO to about 5 mM of phallC6-PDP followed by the addition of pHLIP peptide (2 eq) dissolved in DMSO and incubated at room temperature. More pHLIP was added as needed until almost all phallC6-PDP was reacted. The progress of the reaction was monitored using HPLC (flow rate 1 ml/min; gradient 60 min from 99:1 A/B to 5:95 A/B). Elution times of phallC6-PDP, pHLIP-C6phall and pHLIP were 28.1, 47.2 and 48.5 min, respectively. The pHLIP-C6phall was analyzed using SELDI-TOF (surface-enhanced laser desorption/ionization time-of-flight) mass spectrometry and quantified by measuring OD at 280 and 300 nm. (ε_{280} / ε_{300} of pHLIP and phallacidin is 13940 $M^{-1}cm^{-1}$/2999 $M^{-1}cm^{-1}$ and 10944 $M^{-1}cm^{-1}$/10100 $M^{-1}cm^{-1}$, respectively) MW of pHLIP and pHLIP-C6phall measured/expected were 4122.5/4111.7 Da and 5155.4/5143.0 Da.

Measurements of water-octanol partition coefficient. The polarities of the phallotoxin cargoes were determined by assessment of relative partitioning between aqueous and octanol liquid phases. Constructs dissolved in MeOH:Water 1:1 were added to 0.5 ml of 10 mM phosphate buffer pH 5.5 (saturated with argon) to concentrations of 20 and 30 μM, followed by the addition of argon saturated *n*-octanol

(0.5 ml) and sealed under argon. The solutions were mixed by rotation for 24 hrs at room temperature and left for another 24-48 hrs to reach equilibrium. After phase separation, absorption at 300 nm was recorded. The molar extinction coefficients in *n*-octanol and phosphate buffer are assumed to be the same, and the ratio of the OD readings was used directly to calculate the partition coefficient, $P = OD_{n\text{-octanol}} / OD_{water}$, and Log *P* values. A fraction of aqueous solution was analyzed using HPLC to ensure that no dimers of the phallotoxin was formed.

Liposome preparations

Liposomes were prepared by extrusion: POPC (1-palmitoyl-2-oleoyl-sn-glycero-3-phosphocholine) (500 µl of 10 mg/ml in chloroform) was transferred to a 100 ml round bottom flask and a lipid layer was obtained by evaporating the choloroform in a rotary evaporator, followed by drying under high vacuum for 2 hrs. The lipid layer was resuspended in 10 mM phosphate buffer, pH8, and extruded 31 times through a 50 nm membrane to obtain large unilamellar vesicles.

Measurements of protein fluorescence and circular dichroism (CD) spectroscopic signals

Protein fluorescence and circular dichroism (CD) spectra were measured on a PC1 ISS spectrofluorometer (ISS, Inc.) and a MOS-450 spectrometer (Bioligic, Inc.), respectively, under temperature control. All measurements were performed at 25^{o}C. Peptide fluorescence spectra were recorded from 310 nm to 400 nm using excitation wavelengths of 280 nm. Peptide CD spectra were recorded from 190 nm to 260 nm at

0.5 nm increments using a sample cuvette with an optical path length of 0.5 cm. The following samples were measured: i) pHLIP-C6phall (7 µM) in 10 mM phosphate buffer at pH8, ii) pHLIP-C6phall (7 µM) incubated with POPC liposomes (1.5 mM) in 10 mM phosphate buffer at pH8, and iii) sample (ii) with its pH lowered by the addition of an aliquot of HCl.

Binding assay

Materials and preparation of stock solutions: Rabbit muscle actin was purchased from Cytoskeleton Inc. To obtain polymerized filamentous actin (F-actin), the monomeric globular actin (G-actin) was dissolved in 100 µl of water and incubated for 1 hr at room temperature. After centrifuging at 13,000xg for about 15min, the amount of G-actin in the supernatant was quantified by measuring the OD at 290 nm (ε_{290} of G-actin is 26 600 $M^{-1}cm^{-1}$). G-actin was diluted to 3.5 mg/ml in 2 mM phosphate buffer pH 8 supplemented with 0.2 mM $CaCl_2$ and 0.2 mM ATP and incubated for 1 hr at 4ºC. Polymerization was induced by addition of 50 mM KCl, 2 mM $MgCl_2$ and 1 mM ATP and incubation for 1 hr at room temperature. Texas Red-X phalloidin (PhallTxR) was purchased from Invitrogen Corp. PhallTxR was dissolved in DMF and quantified by measuring OD at 583 nm. (ε_{583} of PhallTx in MeOH is 95,000 $M^{-1}cm^{-1}$). Previously prepared and lyophilized phallotoxins (phallacidin, phallC4SH, phallC6SH and phallC10SH) were dissolved in DMSO and quantified by measuring OD at 300 nm. (ε_{300} of phallotoxins 10,100 $M^{-1}cm^{-1}$).

Binding assay of phallTxR to actin: Samples of 0.6 μM of phallTxR with different F-actin concentrations (from 0 to 6.6 μM) were prepared in polymerizing buffer (2 mM phosphate buffer pH8 containing 50 mM KCl, 2 mM $MgCl_2$, 0.2 mM $CaCl_2$ and 1 mM ATP) and incubated for 2 hrs at room temperature. The fluorescence anisotropy and intensity of each sample were measured with excitation/emission setting at 570 nm/ 610 nm wavelength, respectively under temperature control.

Competition binding assay: The assay is based on titration of 0.3 μM of phallTxR and 0.3 μM of phallotoxin by increasing concentrations of Factin. 10x TCEP was added to 60 μM stock solution of phallotoxins in polymerizing buffer and incubated for 10 min to reduce disulfide bond. Samples of 0.3 μM of phallTxR and 0.3 μM of each phallotoxin were prepared in polymerizing buffer followed by mixing with F-actin to obtain final concentrations of 0, 0.3, 0.6, 1.2 and 2.4 μM of Factin in each sample, and incubated overnight at 4˚C. The fluorescence anisotropy of each sample was measured with excitation/emission setting to 570 nm/ 610 nm measured using PC1 spectrofluorometer under temperature control.

Cell line. Human cervical adenocarcinoma HeLa was purchased from the American Tissue and Culture Collection (ATCC). HeLa was propagated in DMEM (Dulbecco's Modified Eagle Medium) ([+] 4.5 g/L D-glucose, [+] 40 mg/L sodium pyruvate, Gibco) supplemented with 10% FBS (fetal bovine serum) (Gibco), ciprofloxacin-HCl (1 μg/mL) (from Cellgro, Voigt Global Distribution) in a humidified atmosphere of 5% CO_2 at 37^{o}C. HeLa cells were adapted to pH 6.2 by propagation in pH 6.2 DMEM

supplemented with 10% FBS, ciprofloxacin-HCl (1 μg/mL) in humidified atmosphere of 5% CO_2 at 37^{o}C.

Proliferation Assay. Stock solutions of pHLIP-C6phall, phallacidin (control agent) and phallC6SH (control agent) or phalloidin-oleate were prepared in DMSO at 400 μM. A human cervix adenocarcinoma cell line (HeLa) obtained from the ATCC (American Type Culture Collection) was grown at pH 6.2 and 7.4. HeLa cells were seeded in 96-well plates (Costar) at densities of 4000 and 2000 cells per well for treatment on the following day. A DMSO stock of pHLIP-phallC6 (or control agent) was diluted with sterile Leibovitz's L-15 phenol free medium (L-15) pH 5.9 or 7.4 to give treatment solutions in the 0-6 μM range. Appropriate amounts of DMSO were added to ensure that all treatment samples contain the same amount of DMSO by volume (1.5%). After removal of cell media, the L-15 treatment solutions pH 5.9-6.0 or 7.4 (95 μL) were added to cells grown at pH 6.2 and 7.4, respectively, and then the plate was incubated at 37°C for 3 hrs. After treatment, 200 μL of DMEM at pH 6.2 or 7.4 were added to corresponding wells and 10 μl of FBS into each well to provide 10% of FBS in cell medium before returning the plate to the incubator. Cell density of the '0 μM, pH 6.2' and '0 μM, pH 7.4' controls usually reached 80%-90% saturation in well after 4-6 days of growth. The viable cell number was quantified using the MTS reagent (Promega CellTiter 96 AQueous One Solution Cell Proliferation Assay). OD values at 490 nm were obtained using a plate reader (iMark Microplate reader from Bio Rad). Since the rate of cells growth is slightly different at low and neutral pHs, all

numbers were normalized to 100% using wells where no construct was added to the media.

RESULTS

Design and synthesis of phallacidin cargoes of different hydrophobicity

The major goal of our work is to systematically vary the hydrophobicity of a polar cargo, phallatoxin, and to show delivery by a pH-dependent antiproliferative. We chose phallacidin (Figure 1), which is a cyclic cell-impermeable toxin similar to phalloidin and that binds to F-actin with high affinity (*16, 17*). Phallacidin has a free COOH group suitable for conjugation purposes, and we tuned the hydrophobicity of the phallacidin cargo by reacting with diamines NH_2-$(CH_2)_n$-NH_2 with different lengths of hydrophobic chain $(CH_2)_n$, where *n* could be varied from 2 to 12 carbon atoms. We had already tested commercially available phalloidin-oleate, with 15 carbon atoms, which has Log *P* value of +1.7, and observed inhibition of Hela cell proliferation rate by 60%, 70% and 95% after treatment cells with 1, 2 and 4 μM of phalloidin-oleate, respectively, independently of pH (data not shown). Therefore, we selected 3 different lengths of hydrophobic chain diamines, where *n* is 4, 6 and 10 to work with. The phallacidin was conjugated to the various lengths diamines via NHS and DCC crosslinker. We synthesized three phallacidin cargoes with four (phallC4), six (phallC6) and ten (phallC10) carbon atoms. The protocol was adjusted until optimal conditions were established, and the details of the final protocol are in the Methods section. The products were purified using reverse phase C18 HPLC, lyophilized and characterized by ESI mass spectrometry. The molecular weights

obtained for phallacidin cargoes were 917.2 Da for phallC4, 945.2 Da for phallC6 and 1001.2 Da for phallC10 and were very close to expected values(917.1, 945.1 and 1001.2 Da).

Characterization of phallacidin cargoes of different hydrophobicity

To investigate the properties of cargo molecules, they were reacted with SPDP crosslinker, the S-S bond was reduced by TCEP and the reduced cargoes were purified and characterized (see Table 1). The cargo hydrophobicities were evaluated by measuring the logarithm of the octanol-water partition coefficient *P*, calculated based on the amount of constructs distributed upon equilibration between octanol and water phases, measured by the ODs of phallacidin constructs at 300 nm. The Log *P* values of phallacidin and cargoes are presented in Table 1. Phallacidin with a long chain FA of ten carbon atoms is preferably distributed into octanol, being hydrophobic, and shows a positive Log *P* of +1.28. Such molecules should cross cellular membranes by themselves, the hydrophobicity being in the range of conventional drugs. The polarity of phallC6SH with Log *P* = -0.09 was very close to the polarity of phalloidin-rhodamine, which has Log *P* = -0.05 measured previously (*18*). Phallacidin with four carbon atoms, as expected, was the most polar among modified phallacidin cargoes.

According to the literature (*16, 19, 20*) it was expected that modification of COOH group of phallacidin should not affect F-actin binding properties. Phallatoxin binds between actin monomers in filamentous actin and prevents depolymerization (*17, 19*). We used a fluorescence anisotropy titration assay, where phalloidin conjugated to

Texas Red (TxR) fluorescent dye was in competition with phallacidin and cargoes for F-actin binding. The assay is based on the increase of anisotropy of phallTxR when it binds to the F-actin. Samples of equal concentration (0.3 μM) of phallTxR and phallacidin cargoes were prepared with increasing concentrations of F-actin. The samples were incubated overnight, then the fluorescence anisotropy of each sample was measured at 610 nm wavelength with excitation at 570 nm (Figure 2). The anisotropy changes from 0.04 (for unbound phallTxR) up to 0.24 when all phallTxR is completely bound (the value of 0.24 was obtained in separate titration experiment of phalloidinTxR by F-actin in the absence of phallacidin or phallacidin cargoes). Our experiments demonstrate that the anisotropy value in the presence of phallacidin cargoes changes in the same way as anisotropy in the presence of phallacidin, confirming that the attachment of hydrophobic tails to the phallacidin does not alter binding affinity to F-actin.

Synthesis and characterization of pHLIP-*C6*phall

Since phallC6SH has a similar hydrophobicity to rhodamine-phalloidin, we decided to select this cargo, conjugate it to pHLIP, perform spectroscopic characterization and test its anitproliferative properties. PhallC6-PDP was conjugated with single Cys residue at the C-terminus of pHLIP to form a S-S bond. The product was purified using reverse phase C18 HPLC, lyophilized and characterized by SELDI-TOF mass spectrometry (MW of the pHLIP-C6phall was 5155.4 Da) and quantified by measuring OD at 280 and 300 nm.

We have demonstrated previously that changes of intrinsic fluorescence and CD of pHLIP in the presence of liposomes resulting from pH changes is indicative of peptide insertion into the lipid bilayer (*4*, *5*). Here, we carried out spectroscopic characterization of pHLIP-C6phall construct. We observed the characteristic increase of fluorescence signal and shift of the spectrum in presence of POPC liposomes expected from a drop of pH from 8 to 4 (Figure 3a), which indicates that tryptophan residues are buried in the membrane interior due to the peptide partition into bilayer. The construct is predominantly unstructured in aqueous solution and in the presence of POPC at pH8, while helical structure is formed at low pH (Figure 3b). pH induced fluorescence and CD changes seen for pHLIP-C6phall in the presence of lipid bilayers were very similar to those observed for pHLIP alone. Thus, we concluded that conjugation of phallC6SH cargo does not affect the pH-dependent ability of pHLIP to interact with the membrane lipid bilayer.

Antiproliferative effect of pHLIP-C6phall

Finally, we tested the anitproliferative capability of the pHLIP-C6phall construct. HeLa cells were adapted for low pH growth (pH 6.2). Cells grown at low and normal (7.4) pHs were treated with various concentrations of pHLIP-C6phall, phallC6SH and phallacidin in L-15 phenol free medium at pH 6.0 and 7.4 for 3 hrs. After treatment DMEM supplemented with 10% FBS at pH 6.2 or 7.4 was added to corresponding cells. When cell density in the control wells (treated with medium) reached 80%-90% saturation (after 4-6 days of growth) the number of viable cells was quantified using the MTS reagent. Since the rate of cells growth is slightly different at low and neutral

pHs, all numbers were normalized to be 100% where no construct was added to the media. The data clearly demonstrate that pHLIP-C6phall shows antiproliferative effect at low pH of treatment, while at neutral pH no effect is observed (Figure 4). At 2 μM about 60% of cell death was observed at low pH. Phallacidin (as well as phallC6SH) does not demonstrate an antiproliferative effect at either pH.

DISCUSSION

In conventional drug design and discovery the Lipinski rules of five, or subsequently developed similar parameters, are widely used to guide drug designs. The rules postulate that a successful drug should be hydrophobic and small in order to traverse membranes and reach cytoplasmic targets (e.g. the logarithm of the octanol-water partition coefficient Log *P* is -0.4 to +5.6 and the MW is 160 to 480 $g.mol^{-1}$) (*21*). However, the majority of inhibitors found for biological targets located inside a cell are molecules that cannot cross a membrane (*22-24*). We have proposed a novel way to deliver polar molecules across membranes, based on the insertion of a water-soluble, moderately hydrophobic membrane peptide, pHLIP. The spontaneous insertion and folding of the peptide into a lipid bilayer seeks the free energy minimum, and the insertion event is therefore accompanied by a release of energy, which is used to translocate cell-impermeable cargo molecules across a cellular membrane. The Gibbs Free Energy of binding of pHLIP to a POPC surface at 37°C is about -7 kcal/mol near neutral pH and the additional free energy of insertion and folding across a lipid bilayer at low pH is nearly -2 kcal/mol (*12*). The energy difference between membrane-bound and membrane–inserted states favors the partition of cargo across

the hydrophobic barrier of a membrane. Since the energy released during peptide folding and insertion across a membrane is limited, and since strongly polar molecules will reach equilibrium slowly, we assumed that there is a limit on cargo polarity (and most probably on size as well) that can be delivered across a membrane by pHLIP. In support of that, we recently show that pHLIP can move phalloidin across a membrane to inhibit cell proliferation, but only when a hydrophobic facilitator (rhodamine) is attached to the peptide inserting end. In this study we made a first attempt to tune hydrophobicity of polar cargo phallacidin in a systematic manner by conjugation of phallacidin with diamines of different hydrophobic chain lengths. The hydrophobicity of the cargo is modulated by presence of 4 to 10 carbon atoms conjugated to the carboxyl group of phallacidin. The cargoes were synthesized and characterized. We show that the logarithm of the octanol-water partition coefficient (Log *P*) of cargoes was varied from -1.6 for pure phallacidin to +1.28 for phallC10. Cargo to be functional needs to bind to its cellular target,: in the case of phallacidin it is an F-actin. We evaluated the actin-binding ability of cargoes and demonstrated that attachment of a chain of carbon atoms (up to 10 atoms) to the carboxyl group of phallacidin does not affect their ability to interact with F-actin. Since the Log *P* of phallC6SH is very similar to the Log *P* of phalloidin-rhodamine, phallC6SH was selected for testing with pHLIP. The phallC6SH cargo was conjugated via a cleavable S-S bond to the C-terminus of pHLIP, which goes across the membrane. First, we carried out spectroscopic characterization of pHLIP-C6phall cargo. We observed the same as for pHLIP alone characteristic changes of the fluorescence and CD signals, when pHLIP-C6phall interacts with lipid bilayer of a POPC membrane at neutral and low pHs. It

was an important sign, indicating that attachment of phallC6SH cargo to the inserting end of the peptide does not alter its pH-dependent membrane interaction. Next, we carried out cell experiments to demonstrate that phallC6SH could be translocated across a membrane by pHLIP to induce inhibition of cell proliferation. It is known that phallacidin in the cytoplasm stabilizes actin in its filamentous form, preventing depolymerisation. Since cell movement and shape changes are associated with actin polymerization/depolymerisation, stabilization of F-actin depolymerisation leads to the freezing of cell movement, formation of multinucleated cells and eventually cell death (*8, 18*). Phallacidin and phallC6SH are too polar to diffuse themselves across membrane in sufficient amount to induce any biological effect, while pHLIP facilitates translocation of phallC6SH at slightly acidic pH, which in turns inhibits cell proliferation in a concentration-dependent manner.

In contrast to all other known peptide-based delivery technologies, selective delivery of molecules into the cytoplasm by pHLIP is achieved by the pH-dependent folding of a monomeric peptide across the plasma membrane. In response to the low extracellular pHs of cells in diseased tissues, pHLIP can translocate polar therapeutic cargo molecules into cell cytoplasms, whereas at the normal extracellular pH of healthy tissue, only a minimal translocation of cargo across cell membranes would occur. Because the cargo is translocated across a cell membrane directly into the cytoplasm, endosomal trapping is avoided. Tuning the cargo hydrophobicity can be used to achieve the maximum difference between the therapeutic effect at low pH versus at

neutral pH, thereby enhancing diseased-targeted delivery and reducing treatment side effects.

ACKNOWLEDGMENT. This work was supported by NIH grant CA133890 to OAA, DME, YRK, and by DoD grant PC050351 to YKR. We thank Dr. Anna Moshnikova and Erin Jansen (Physics, URI) for help with cells experiments and purification of constructs, respectively; Prof. Brenton DeBoef and Dr. Shathaverdhan Potavathri (Chemistry, URI) for guidance in phallcidin cargo synthesis; Dr. Ming An (Molecular Biophysics and Biochemistry, Yale), Dr. Gregory Watkins (Delpor, Inc.) for discussion.

FIGURES

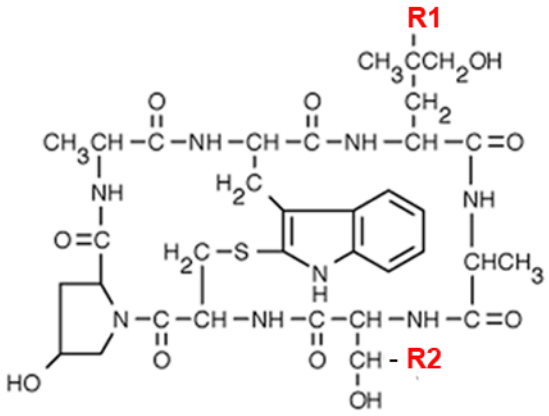

Figure 1. Chemical structures of cyclic peptides: phalloidin, where R1 = OH and R2 = CH_3; phallodin-rhodamine where R1 = rhodamine; and phallacidin, where R1 = H and R2 = COOH.

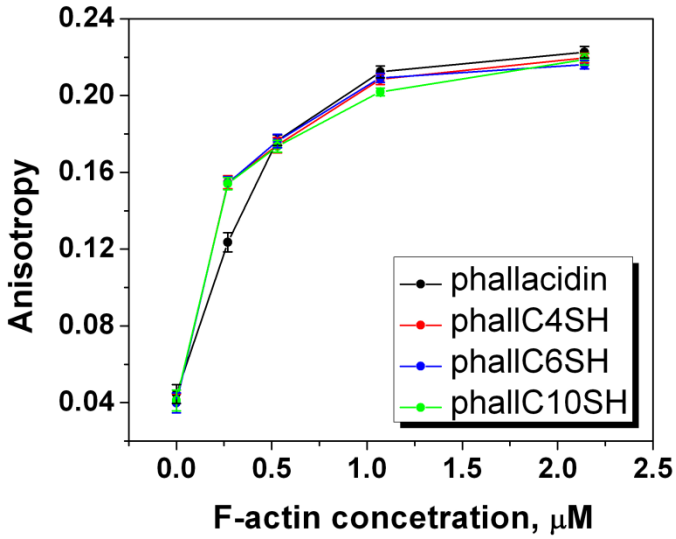

Figure 2. Binding competition assay. Changes of fluorescence anisotropy of Texas Red conjugated to phalloidin was monitored in the presence of phallacidin or phallacidin cargoes at different F-actin concentrations.

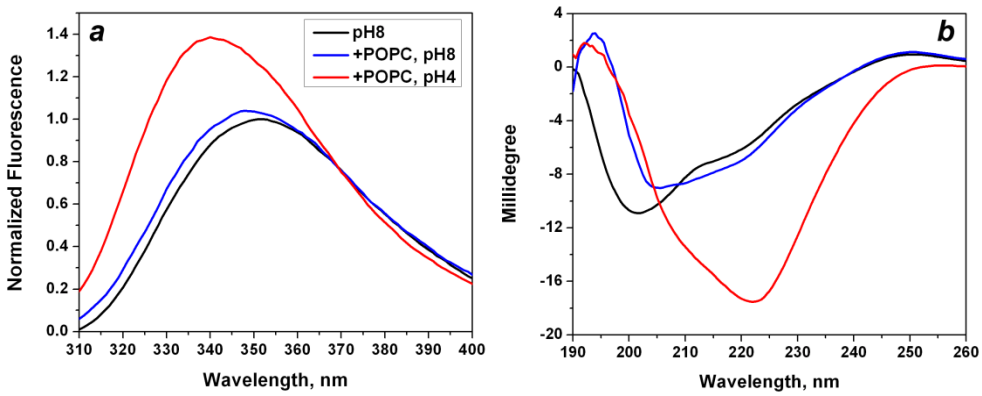

Figure 3. Changes of tryptophan fluorescence (***a***) and CD (***b***) spectral signals upon pHLIP-C6phall interaction with POPC liposomes at various pHs. Black lines represent spectra for the construct in aqueous solution at pH8, Blue lines upon incubation with POPC liposomes at pH8, and red lines after the pH was dropped from 8 to 4.

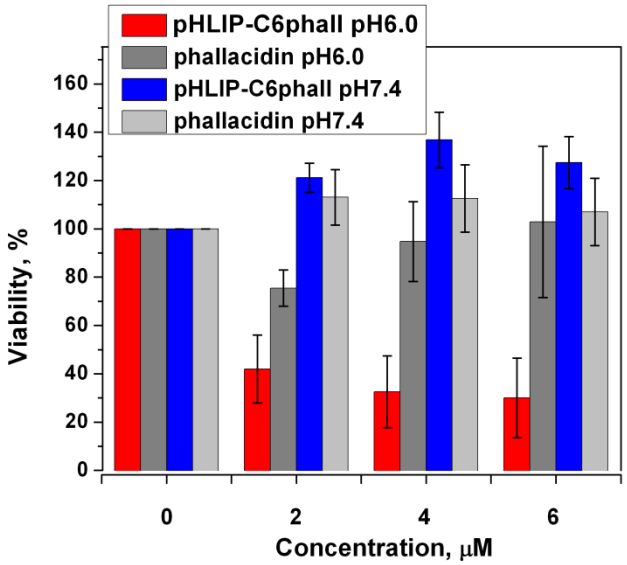

Figure 4. Inhibition of cell proliferation by pHLIP-C6phall at pH6. There is no significant effect observed at pH 7.4.

TABLES

Table 1. Characterization of phallacidin and phallalacidin-C4, -C6 and –C10 cargoes: percentage of acetonitrile of cargo elutions from the column and the logarithms of the octanol-water partition coefficients (Log *P*).

	Acetonitrile, %	**Log *P***
phallacidin	20.3	-1.6
phallC4SH	22.4	-0.74
phallC6SH	25.5	-0.09
phallC10SH	34.4	+1.28

REFERENCES

1. Jeffrey, S. S., Lonning, P. E. and Hillner, B. E. (2005) Genomics-based prognosis and therapeutic prediction in breast cancer, *J. Natl. Compr. Canc. Netw. 3*, 291-300.

2. Krebs, H. A. (1972) The Pasteur effect and the relations between respiration and fermentation., *Essays Biochem. 8*, 1-34.

3. Warburg, O., Wind, F. and Negelein, E. (1927) The metabolism of tumors in the body, *J. Gen. Physiol. 8*, 519-530.

4. Hunt, J. F., Rath, P., Rothschild, K. J. and Engelman, D. M. (1997) Spontaneous, pH-dependent membrane insertion of a transbilayer alpha-helix, *Biochemistry 36*, 15177-15192.

5. Reshetnyak, Y. K., Segala, M., Andreev, O. A. and Engelman, D. M. (2007) A monomeric membrane peptide that lives in three worlds: in solution, attached to, and inserted across lipid bilayers, *Biophys. J. 93*, 2363-2372.

6. Andreev, O. A., Engelman, D. M. and Reshetnyak, Y. K. (2009) Targeting acidic diseased tissue: New technology based on use of the pH (Low) Insertion Peptide (pHLIP), *Chim. Oggi. 27*, 34-37.

7. Andreev, O. A., Engelman, D. M. and Reshetnyak Y. K. . (2010) pH-sensitive membrane peptides (pHLIPs) as a novel class of delivery agents, *Mol. Membr. Biol. 27*, 341-352.

8. Reshetnyak, Y. K., Andreev, O. A., Lehnert, U. and Engelman, D. M. (2006) Translocation of molecules into cells by pH-dependent insertion of a transmembrane helix, *Proc. Natl. Acad. Sci. U. S. A. 103*, 6460-6465.

9. Thevenin, D., An, M., and Engelman, D. M. (2009) pHLIP-mediated translocation of membrane-impermeable molecules into cells, *Chem. Biol. 16*, 754-762.

10. Andreev, O. A., Dupuy, A. D., Segala, M., Sandugu, S., Serra, D. A., Chichester, C. O., Engelman, D. M. and Reshetnyak, Y. K. (2007) Mechanism and uses of a membrane peptide that targets tumors and other acidic tissues in vivo, *Proc. Natl. Acad. Sci. U. S. A. 104*, 7893-7898.

11. Musial-Siwek, M., Karabadzhak, A., Andreev, O. A., Reshetnyak, Y. K. and Engelman, D. M. (2010) Tuning the insertion properties of pHLIP, *Biochim. Biophys. Acta 1798*, 1041-1046.

12. Reshetnyak, Y. K., Andreev, O. A., Segala, M., Markin, V. S. and Engelman, D. M. (2008) Energetics of peptide (pHLIP) binding to and folding across a lipid bilayer membrane, *Proc. Natl. Acad. Sci. U. S. A. 105*, 15340-15345.

13. Andreev, O. A., Karabadzhak, A. G., Weerakkody, D., Andreev, G. O., Engelman, D. M. and Reshetnyak, Y. K. (2010) pH (low) insertion peptide (pHLIP) inserts across a lipid bilayer as a helix and exits by a different path, *Proc. Natl. Acad. Sci. U. S. A. 107*, 4081-4086.

14. Vavere, A. L., Biddlecombe, G. B., Spees, W. M., Garbow, J. R., Wijesinghe, D., Andreev, O. A., Engelman, D. M., Reshetnyak, Y. K. and Lewis, J. S. (2009) A novel technology for the imaging of acidic prostate tumors by positron emission tomography, *Cancer Res. 69*, 4510-4516.

15. Reshetnyak, Y. K., Yao, L., Zheng, S., Kuznetsov, S., Engelman, D. M. and Andreev, O. A. (2010) Measuring Tumor Aggressiveness and Targeting Metastatic Lesions with Fluorescent pHLIP, *Mol. Imaging Biol. 107*, 20246-20250.

16. Wieland, T. (1977) Modification of actins by phallotoxins, *Naturwissenschaften 64*, 303-309.

17. Barak, L. S. a. Y., R. R. (1981) 7-Nitrobenz-2-oxa-1,3-diazole (NBD) - phallacidin: synthesis of a fluorescent actin probe, *Anal. Biochem. 110*, 31-38.

18. An, M., Wijesinghe, D., Andreev, O. A., Reshetnyak Y. K. and Engelman, D. M. (2010) pH-(low)-insertion-peptide (pHLIP) translocation of membrane impermeable phalloidin toxin inhibits cancer cell proliferation, *Proc. Natl. Acad. Sci. U. S. A. 107*, 20246-20250.

19. Wieland, T., Hollosi, M. and Nassal, M. (1983) Components of the green deathcap mushroom (Amanita phalloides), LXI: delta-Aminophalloin, a 7-analogue of phalloidin, and some biochemically useful, including fluorescent derivatives, *Liebigs. Ann. Chem. 1983*, 1533-1540.

20. Falcigno, L., Costantini, S., D'Auria, G., Bruno, B. M., Zobeley S., Zanotti, G. and Paolillo, L. (2001) Phalloidin synthetic analogues: structural requirements in the interation with F-actin, *Chem. Eur. J. 7*, 4665-4673.

21. Lipinski, C. A., Lombardo, F., Dominy, B. W. and Feeney, P. J. (2001) Experimental and computational approaches to estimate solubility and permeability in drug discovery and development settings, *Adv. Drug Deliv. Rev. 46*, 3-26.

22. Tsutsumi, S. a. N., L. (2007) Extracellular heat shock protein 90: a role for a molecular chaperone in cell motility and cancer metastasis, *Cancer Sci. 98*, 1536-1539.

23. Wang, J. L., Zhang, Z. J., Choksi, S., Shan, S., Lu, Z., Croce, C. M., Alnemri, E. S., Korngold, R. and Huang, Z. (2000) Cell permeable Bcl-2 binding peptides: a chemical approach to apoptosis induction in tumor cells, *Cancer Res. 60*, 1498-1502.

24. Sun, H., Nikolovska-Coleska, Z., Yang, C. Y., Qian, D., Lu, J., Qiu, S., Bai, L., Peng, Y., Cai, Q. and Wang, S. (2008) Design of small-molecule peptidic and nonpeptidic Smac mimetics, *Acc. Chem. Res. 41*, 1264-1277.

CHAPTER 3

In the process of submission to Biophysical journal

Membrane-associated folding:

II. Polar cargo translocation across a lipid bilayer

Dayanjali Wijesinghe[1], Alexander G. Karabadzhak[1], Vladislav S. Markin[2], Donald M. Engelman[3], Oleg A. Andreev[1], Yana K. Reshetnyak[1]

[1]Physics Department, University of Rhode Island, 2 Lippitt Rd., Kingston, RI, 02881, USA

[2] Department of Neurology, University of Texas Southwestern Medical Center, Dallas, TX, 75390-9036, USA

[3]Department of Molecular Biophysics and Biochemistry, Yale University, P.O. Box 208114, New Haven, CT 06520, USA

Running title: Cargo translocation across a bilayer

Keywords: pH Low Insertion Peptide (pHLIP), pH-sensitive, single peptide molecular transporter, drug delivery, kinetics

Corresponding author:

Yana Reshetnyak, Physics Department, University of Rhode Island, 2 Lippitt Rd., Kingston, RI, 02881, USA, Phone: (401) 874-2060, Fax: (401) 874-2380, E-mail: reshetnyak@mail.uri.edu

ABSTRACT

Here we present the results of the study of the mechanism of cargo translocation across a membrane by the single molecule transporter, pHLIP® (pH (Low) Insertion Peptide). The main principle of this novel drug delivery approach is based on the phenomenon of the pH-dependent insertion and folding of moderately hydrophobic membrane peptides. Several pHLIP variants were used to probe the delivery of cargoes of different polarities (biotin and biotin-Peg) attached to the peptide inserting end. We confirm that all pHLIP variants with attached cargo molecules preserve the pH-dependent properties of interaction with a membrane. While the equilibrium thermodynamics favor the binding and insertion of the pHLIP-cargo constructs, the kinetics was significantly slowed down. The presence of a polar cargo at the peptide's inserting end leads to the appearance of two additional intermediate states on the insertion pathway of the pHLIP-2E, which itself (when no cargo is attached) shows an all-or-none transition from the partially unstructured membrane-surface state to the transmembrane state described very well by the two-state model. Our findings are very valuable for the design of new delivery agents for the direct translocation of polar cargo across a membrane. To facilitate the different delivery needs for different applications the hydrophobicity of the cargo could be modified without affecting the cargo's ability to bind to its cellular target (shown by us previously) and/or various peptides of the pHLIP family could be employed, which show different rates and pKa of a cargo's translocation across cellular membranes.

INTRODUCTION

The transportation of molecules across a membrane is a vital property of a cell. Cells can transport molecules by various mechanisms. The number of molecules that can freely diffuse across a cellular membrane is very limited since the energetic barrier for transitions across the hydrophobic lipid bilayer of a membrane is very high for polar molecules. The endocytotic mechanisms are very effective; however, there is a problem of escaping from endosomes, which is one of the main obstacles for the delivery of drugs into cells.

Recently we have discovered that a moderately hydrophobic, water-soluble membrane peptide pHLIP (pH (Low) Insertion Peptide) can insert into membranes and translocate molecules in a pH-sensitive manner (1, 2). The mechanism of the membrane insertion and folding of pHLIP is based on the protonation of the carboxyl groups of Asp/Glu residues, which results in an enhancement of the peptide's hydrophobicity and increase its affinity for a lipid bilayer, triggering the peptide to fold and subsequently to insert into the membrane (3, 4). The energy of membrane associated-folding of about 2 kcal/mol could be used to move polar cell-impermeable cargo molecules attached to the inserting end of the pHLIP through the hydrophobic bilayer of a membrane (5). Both, pH-targeting behavior and molecular translocation have been proven on cultured cells and *in vivo* (3, 6-10). Among the polar cargo molecules that have been successfully translocated into the cytoplasm are fluorescent dyes, a gene regulation agent - peptide nucleic acid, a toxin –phalloidin conjugated with fluorescent dye rhodamine (6), cyclic peptides (7), phalloidin, when the facilitator group, rhodamine, was attached to the inserting end of the pHLIP (10),

phallacidin (another version of the toxin) with six carbon groups attached to it (11). Thus, it opens an opportunity to develop a novel concept in drug delivery, which is based on the use of a pH-sensitive single peptide molecular transporter.

The thermodynamic and kinetic studies provide understanding of the mechanism of pHLIP's interaction with the lipid bilayer of a membrane. The results of the kinetic studies presented in the first manuscript of this series indicate that the rate of the peptide insertion into a membrane could be enhanced 10 and even 100 times if charged groups are removed from the inserting end of the peptide (12). The main goal of this study is to elucidate the mechanism of cargo translocation across a bilayer by a family of pH-sensitive single peptide molecular transporters, pHLIPs. As a cargo we used biotin and biotin-Peg, which were attached to the C-terminus of several pHLIP variants including truncated (fast) pHLIPs.

MATERIALS AND METHODS

Conjugation of biotin and biotin-peg to the pHLIPs

The pHLIP peptides were prepared by solid-phase peptide synthesis at the W.M. Keck Foundation Biotechnology Resource Laboratory at Yale University. The lyophilized powder was soluble in 3 M urea or DMSO (dimethyl sulfoxide). When dissolved in urea the peptide was transferred to a buffer using a G-10 size-exclusion spin column. The concentration of the peptide was determined spectrophotometricly by measuring the absorbance at 280 nm (ε_{280}=13,940 $M^{-1}cm^{-1}$). For conjugation with biotin and biotinPeg, pHLIP peptides were mixed with the biotin-maleimide or biotin-$dPeg_3$-maleimide (Quanta Biodesign Ltd) in DMSO in a ratio of 1:10 and incubated at room

temperature for about 8 hrs and at 4ºC until the conjugation reaction was completed. The reaction progress was monitored by HPLC. The product was purified using reverse phase C18 HPLC, lyophilized and characterized by SELDI-TOF mass spectrometry.

Measurements of water-octanol partition coefficient

The polarity of biotin-maleimide and Peg-biotin-maleimide was determined by the assessment of the relative partitioning between the aqueous and octanol liquid phases. The biotin and biotin-Peg was dissolved in a 10 mM phosphate buffer pH8 (0.5 ml) at concentrations of 3 and 5 mM (for biotin), 10 and 50 mM (for biotin-Peg) followed by the addition of *n*-octanol (0.5 ml). The solutions were mixed by rotation for 24 hrs at room temperature and then left for another 48 hrs in order to reach an equilibrium. After the phase separation, the absorption at 300 nm was recorded. The molar extinction coefficients in *n*-octanol and phosphate buffer are assumed to be the same, and the ratio of the OD readings was used directly to calculate the partition coefficient, P = OD*n*-octanol/ODwater, and Log P values, which reflects the relative polarity of cargo.

Liposomes preparation

Liposomes were prepared by extrusion: POPC (1-palmitoyl-2-oleoyl-sn-glycero-3-phosphocholine) (700 µl of 10 mg/ml in chloroform) was transferred to a 100 ml round bottom flask and a lipid layer was obtained by evaporating the choloroform in a rotary evaporator, followed by drying under a high vacuum for 2 hrs. The lipid layer

was resuspended in a 10 mM phosphate buffer, pH8, and extruded 31 times through 50 or 100 nm membrane to obtain large unilamellar vesicles.

Steady state fluorescence and CD measurements

The protein's fluorescence and circular dichroism (CD) spectra were measured on a PC1 ISS spectrofluorometer (ISS, Inc.) and a MOS-450 spectrometer (Bioligic, Inc.), respectively, under temperature control at 25^{o}C. 7 μM of peptide and 1.5 mM of POPC in 10 mM phosphate buffer pH8 were pre-incubated overnight at 4ºC. The three states were monitored by the changes of the fluorescence and CD. The fluorescence spectra of the pHLIP variant were recorded with the excitation at 280 nm and used polarizers in the excitation (magic angle) and emission (vertical) light paths. We chose a 280 nm excitation wavelength instead of 295 nm in order to reduce the absorbance of biotin that is centered at 300 nm (which is significantly lower than the absorbance of the peptides). The peptide's CD spectra were recorded from 190 nm to 260 nm at 0.5 nm increments using a sample cuvette with an optical path length of 0.5 cm.

Stopped-flow fluorescence measurements

The stopped-flow fluorescence measurements at different temperatures were carried out using a SFM-300 mixing apparatus connected to a MOS-450 spectrometer. The FC-20 observation cuvette was used for the fluorescence measurements. All solutions were degassed for several minutes under a vacuum before loading them into the syringes to minimize air bubbles. The pHLIP variants (7 μM) were pre-incubated with POPC (1.5 mM) at pH 8.0 to reach a binding equilibrium and the folding/insertion

was induced by the fast mixing (5 ms dead time) of equal volumes of pHLIP-POPC variants at pH 8.0 and appropriately diluted with HCl, to obtain a drop of pH from 8 to 3.6. The changes of the pHLIP fluorescence signal were recorded through a 320 nm cutoff filter using an excitation wavelength of 280 nm. The fluorescence signal was corrected for the photobleaching. Each kinetic curve was recorded several times and then averaged, excluding the first 3–4 shots.

pH dependence study

Solutions of pHLIP-2-bt and pHLIP-2E-bt were mixed with POPC to obtain 200 µl of 3 µM of the peptide and 2 mM POPC in a pH8 phosphate buffer. The pH of the peptide/lipid samples were dropped by addition the of HCL and left for about 5 min for equilibration. The pH was measured by a micro-electrode probe (Orion 8220B). The fluorescence spectra at an excitation of 280 nm were recorded at each pH value under a constant temperature. The spectra were analyzed by the decomposition algorithms (13) using the on-line PFAST toolkit (Protein Fluorescence And Structural Toolkit: http://pfast.phys.uri.edu/) (14) to establish the position of the maximum. Finally, the position of the maximum of the fluorescence spectra (λ_{max}) versus the pH was plotted and the Henderson–Hasselbalch equation was used to fit the data (using Origin 8.5 software):

$$\lambda_{max} = \lambda^2_{max} + \frac{(\lambda^1_{max} - \lambda^2_{max})}{1 + 10^{n\cdot(pH-pKa)}}$$

where λ^1_{max} and λ^2_{max} are the beginning and end of the transition, *n* is the cooperativity parameter, and *pK*a – is the mid of transition, which we are looking to estimate.

Data analysis

Nonlinear least squares curve fitting procedures were carried out in Origin 8.5.

RESULTS

We elucidated the molecular mechanism of pHLIP peptides interaction with lipid bilayer of membrane. Also, we proved that a polar cell-impermeable cargo could be moved across a bilayer by the pHLIP in a pH-dependent manner. The main goal of this study is to gain mechanistic insights into the process of cargo translocation by various pHLIP variants. In the previous manuscript of this series we demonstrated that the removal of the protonatable carboxyl groups from the inserting C-terminus of the pHLIP significantly increases the rate of the peptide's insertion into a membrane. Also, in our previous studies we showed that the pKa of the original pHLIP was shifted from 6.0 to 6.5 when an Asp residue in the TM domain was replaced by a Glu (4). For the cargo delivery applications, a higher pKa and rate of the peptide insertion are more appealing because the amount of cargo molecules that are translocated into cells are expected to be higher.

We selected the following pHLIP sequences for the investigation with cargo:

pHLIP-4: AE-QN-PI YWARYADWLFTTPLLLLDLALLV DADEGCT-COOH

pHLIP-2: AEDQN-PI YWARYADWLFTTPLLLL*D*LALLV *DC*--G-T-COOH

pHLIP-2E: AEDQNDPI YWARYADWLFTTPLLLL*E*LALLV *E*C--G-T-COOH

The pHLIP-4 is an original pHLIP sequence used for the translocation of various cargo molecules (6, 7, 10). The pHLIP-2 is a truncated version of the pHLIP-4, containing just two carboxyl groups at the inserting end, which shows 10 times faster propagation into membrane in comparison to the pHLIP-4 in a result of pH drop from 8 to 3.6. The pHLIP-2E is a pHLIP-2 where two Asp residues were replaced by Glu to increase pKa of the peptide insertion into a membrane. The Asp residues that were removed from the C-terminus were placed at the N-terminus to preserve the peptide's solubility. All the pHLIP variants had a free SH group at the C-terminus for the conjugation with maleimide-cargo molecules. As cargo we chose biotin and biotin-Peg mainly due to their Log *P* values, the convenience of their conjugation to the peptide and low level of absorbance and no fluorescence in UV range (in contrast to fluorescent dyes). The measured Log *P* of biotin and biotin-Peg are -0.29 and -1.39, respectively (for the comparison Log *P* of phalloidin and phalloidin-rhodamine is -1.5 and -0.05, respectively, (10)). We have shown previously that the pHLIP-4 is capable of translocating biotin-Peg (15), as well as other polar cargoes of similar polarity (7). All constructs were purified to remove all un-reacted peptide and cargo.

We employed the fluorescence and CD spectroscopic techniques to probe the pHLIPs-cargo construct's interaction with the lipid bilayer of POPC liposomes. The three states were measured for the pHLIPs-biotin (pHLIP-bt) and the pHLIPs-biotin-Peg (pHLIP-btPeg) as well as for the pHLIP-2E. The fluorescence and CD spectra of the pHLIP variants with cargoes at normal and low pH in the absence and presence of POPC liposomes are shown in the Figures 1 and 2. The spectral parameters are summarized in the Table 1. All pHLIP-cargo constructs demonstrate the characteristic

three states. At pH8 in the absence of liposomes (state I) all pHLIP-cargo constructs are mostly unstructured (characteristic negative band on CD spectra at 195 nm) with fluorophores exposed to the aqueous solution (the maximum of fluorescence is at 350-352 nm). The addition of the POPC liposomes at pH8 (state II) leads to the increase of the fluorescence quantum yield along with the blue shift of the position of maximum of emission spectra, which reflects the peptide-cargoe's attachment to the lipid bilayer and its partial partition into the membrane. At low pH4 (state III) further increase of the fluorescence intensity and an additional blue shift of the emission spectra were observed for all pHLIP-cargo constructs. The peptide-cargo partition into membrane is accompanied by the formation of helical structure (minima at 208 and 225 nm on CD spectra).

We noticed that the pHLIP variants with attached cargoes demonstrate less increase of the fluorescence in the state II as compared to that of the corresponding peptides with no cargo. The polarity of the cargo attached to the truncated pHLIP variants (-2 and 2E) correlates with the shift of the position of the maximum of the fluorescence to the longer-wavelengths in the state II, which tells us that the emitting residues have a higher exposer to the solvent. An especially significant shift of the fluorescence was observed for the pHLIP-2E peptide, the position of the maximum of the emission spectra shifts from 341.3 nm (for pHLIP-2E) to 344.7 nm (for pHLIP-2E-bt) and 347.9 nm (for pHLIP-2E-btPeg). The emission is shifted from 345.6 nm (for pHLIP-2-bt) to 347.5 nm (for pHLIP-2-btPeg). The fluorescence of the pHLIP-4 and its cargo constructs is a long-wavelength and positioned around 349 nm. The amount of helical structure presented in molar ellipticity (θ) at 225 nm, which usually correlates with the

peptide's partition into membrane, is also reduced from -2.41 to -1.43 for the pHLIP-2-bt and –btPeg, and from -4.42 to -3.96 to -2.27 for the pHLIP-2E, -2E-bt and -2E-btPeg. The obtained data indicate that the peptides (especially pHLIP-2 and 2E, which are more hydrophobic and partition into the membrane deeper and have higher helicity content at pH8 as compared to the pHLIP-4) are pulled up by the polar cargo molecules attached to their C-terminus. The higher that the cargo polarity (negative Log *P* values) is that is attached to the pHLIP, the less the constructs partition into the membrane, which is accompanied by a reduction in the helicity. The same tendency is observed for the state III. The quantum yield and the helicity content is slightly reduced for the pHLIP variants with cargo as compared to them without attached cargo. Even though the obtained steady-state fluorescence and CD data could not provide a quantitative measure of the amount of the cargo translocated across a lipid bilayer, however these data indicate that the attachment of a polar cargo reduces the number of peptide molecules reaching state III. Moreover, the polarity of a cargo most probably correlates with the amount of its translocation across a bilayer.

We also investigated how the attachment of a polar (not charged) cargo might affect the pKa of the peptide-cargo construct's insertion into a membrane. We performed a pH dependence study of the pHLIP-2-bt and pHLIP-2E-bt. Figure 3 demonstrates shift of the position of the maximum of the emission of the pHLIP-2-bt and pHLIP-2E-bt as a function of the pH. The pKa of the transition was found by the fitting of the curves with the Henderson–Hasselbalch equation (see Method section). The pKa of membrane-insertion for the pHLIP-2-bt and pHLIP-2E-bt is 6.0 and 6.8, respectively. The pKa of the pHLIP-2 was found to be 6.1 (12) and the pKa=6.5 for the original

pHLIP (pHLIP-4), where a single Asp residue from the TM domain was replaced by a Glu (4). Slightly higher value of the pKa for the pHLIP-2E-bt could be explained by the fact that two Asp residues were replaced by a Glu, which have higher pKa of protonation.

The obtained results show that a cargo does not affect the pH-dependent ability of the pHLIPs to insert into a membrane much. The amount of the inserted peptides correlate in some degree with its cargo's polarity: the more polar the cargo is, the slightly less the peptide will insert into the membrane. However, the changes are not dramatic. Next we proposed to address the question of a cargo influence on the kinetics of the pHLIP's insertion into a membrane. We performed fluorescent kinetics studies of the pHLIPs and pHLIP-cargo constructs insertion into a membrane. The pHLIP variants were pre-incubated with POPC liposomes at pH 8 to ensure that an equilibrium in the state II was reached, and after a rapid mixing with HCl to reduce the pH from 8 to 3.6, the changes of the fluorescence were measured in real time. The figure 4 demonstrates that the attachment of the biotin cargo to peptides slows down the process of insertion of the pHLIP-4 and pHLIP-2 by 20 and 4 times, respectively. Note that the rate of insertion of the pHLIP-2 is 10 times higher compared to the pHLIP-4 (the details of the study could be found in the first manuscript of this series). Thus the cargo's attachment in more a significant degree affects the kinetics of the peptide's insertion rather than its thermodynamics.

To gain more insights in the process of the peptide-cargo insertion into a membrane we recorded the kinetics of insertion for the pHLIP-2E, pHLIP-2E-bt and pHLIP-2E-btPeg at different temperatures. We concentrated our attention on the pHLIP-2E and

cargoes attached to it, since it is the most interesting pHLIP sequence from the point of view of cargo delivery to the cytoplasm, and there are no kinetics data presented for this pHLIP variant in the previous study. The insertion of the pHLIP-2E without and with cargoes into the lipid bilayer was triggered by the drop of the pH from 8 to 3.6, and the increase of the fluorescence was monitored at different temperatures (25, 18, 11, 7ºC) (Figure 5 *a*-*c*). It could be noted that the attachment of cargo slows the process of peptide insertion about 100 times.

To obtain the rate constants we applied the same mathematical formalism as described in the previous study. The kinetic curves of the pHLIP-2E were adequately fitted by the single exponential function:

$$F(t) = f_0 + f_1 \exp(-t/\tau_1) \quad (1)$$

where τ_i are the characteristics time for each transition or $v_i = 1/\tau_i$ are the characteristic rates of the transitions, and f_i are the characteristics contributions. The single exponential function is a general solution for the two-state (no intermediates) model:

$$\mathrm{A} \underset{k_1^-}{\overset{k_1}{\rightleftharpoons}} \mathrm{B}$$

However, to describe the kinetic of the pHLIP-2E-bt and –btPeg, a three-exponential function was used:

$$F(t) = f_0 + f_1 \exp(-t/\tau_1) + f_2 \exp(-t/\tau_2) + f_3 \exp(-t/\tau_3) \quad (2)$$

which is a general solution of the four-state (two intermediates) model:

$$\mathrm{A} \underset{k_1^-}{\overset{k_1}{\rightleftharpoons}} \mathrm{B} \underset{k_2^-}{\overset{k_2}{\rightleftharpoons}} \mathrm{C} \underset{k_3^-}{\overset{k_3}{\rightleftharpoons}} \mathrm{D}$$

As we already demonstarted in the previous paper (see Appendix 1-3 in (12)) by making a number of assumptions, simple approximate relations between the rate

constants *k* and the characteristic rates, *v*, obtained in a result of the exponential fitting of the experimental data, could be established. For the two-state model:

$$k_1 \sim 0.91 v_1, \quad (3)$$

and for the four-state model:

$$k_1 \sim v_1, \qquad k_2 \sim \frac{v_2}{1.1} - \frac{v_3}{12.21}, \qquad k_3 \sim 0.991 v_3 \quad (4)$$

The fitting of the kinetic curves of the pHLIP-2E-bt and –btPeg was performed with fixed characteristic times as established by the fitting of the pHLIP-2E kinetic data. The characteristic times and rate constants are given in the Table 2. When cargo is attached to the inserting end of the peptide the process of insertion into membrane slows down from 200-400 ms (no cargo) to 80-130 sec (with cargo). It is interesting to note, that there is no significant difference in the kinetic of insertion between the pHLIP conjugated with biotin and biotin-Peg cargoes.

To establish activation energies (E_a) and frequency factors (*A*) for the transitions between states for the pHLIP-2E without and with cargoes, several Arrhenius plots were constructed (Figure 5*d*). The points were fitted by the Arrhenius equation (red lines on Figure 5*d*):

$$\ln k = -E_a/RT + \ln A \quad (5)$$

A global fit was applied for the analysis of the second transition of the pHLIP-2E-bt and –bt-Peg, and third transition for the same constructs. The thermodynamic activation parameters are shown in the Table 3. The activation energy barrier and frequency factor for the pHLIP-2E is 6 kcal/mol and 1.1×10^5, respectively. Two additional steps appear on the pathway of insertion for the pHLIP-2E-bt and –btPeg.

The second and third transitions have activation energy barriers of 9.7 and 3.9 kcal/mol, respectively. The frequency factors for the pHLIP-cargo transition from the first intermediate to the second one, are million times higher than the frequency factor for the transition to the final state. It might reflect the fact that at a final stage of the peptide propagation into a membrane to adopt TM orientation and move cargo across a bilayer, the process could be slowed down significantly.

DISCUSSION

Many approaches to targeted delivery are currently under development, each with its comparative advantages and disadvantages (16, 17). In contrast to all known peptide-based delivery technologies, the selective delivery of molecules across a membrane by the pHLIP is achieved by the pH-dependent folding of the peptide across a bilayer. The pHLIP could be viewed as a single molecule transporter. The partition of the pHLIP into the outer leaflet of lipid bilayer at neutral pH and the folding/insertion at low pH are accompanied by the release of energy. We found that the Gibbs Free Energy of binding to a POPC surface (state I - state II transition) at 37°C is about -7 kcal/mol near neutral pH and the additional free energy of insertion and folding across a lipid bilayer at low pH (state II - state III transition) is nearly -2 kcal/mol (5). The energy difference between the state II and state III is used to favor the equilibrium partitioning across the hydrophobic bilayer of a membrane. We already proved that the pHLIP can translocate various polar molecules across a cellular membrane in a pH-dependent manner (6, 7, 10). This study was designed with the main aim being to gain

an understanding of the mechanism of cargo translocation, which would allow us to tune the pHLIP's properties and improve its cargo delivery.

We choose biotin and biotin-Peg as polar cargo molecules of different polarity. The cargoes were attached to the inserting end of several pHLIP variants to probe the pHLIP-cargo constructs interaction with membrane. Among the investigated pHLIP variants were the pHLIP-4, pHLIP-2 and pHLIP-2E. The pHLIP-4 was used in all cargo translocation experiments. It has four protonatable residues at the inserting end. The pHLIP-2 and 2-E are truncated versions of the pHLIP-4, with two protonatable groups at the C-terminus. Two Asp residues were replaced by a Glu in the pHLIP-2E to increase the pKa of protonation and a peptide's insertion into a membrane.

The steady-state fluorescence and CD measurements indicate that the attachment of cargo does not affect the peptides ability to interact with a lipid bilayer in a pH-dependent manner. The pHLIP-2-biotin has the similar pKa of insertion into membrane as the pHLIP-2. Thus, as we expected, non-protonatable cargo does not change the pKa of insertion. At the same time, the pKa of the insertion of the pHLIP-2E-bt was shifted to 6.8 due to the replacement of two Asp by Glu residues.

The attachment of polar cargoes alters the state II of the peptides (peptide bound to the membrane at neutral and high pHs). The pHLIP-2 and especially pHLIP-2E, demonstrated a deeper positioning in the membrane as compared to the pHLIP-4, due to the fewer number of charged groups at the C-terminus. Polar cargo attached to the C-terminus creates a "pulling" force ($\vec{F}_{out}$) that is directed out from the membrane core (Figure 6) and, as a result the pHLIP-2 and -2E peptides adopt a more exposed position to the solvent at the membrane surface. We assume that the affinity to the

membrane in the state II of the peptides with polar cargo is slightly lower as compared to the affinity of the peptides with no cargo. The higher the polarity of the cargo is, the less the binding affinity that might be observed is. The spectral properties of the pHLIP-cargo constructs in the state III are just slightly different as compared to those of the pHLIP peptides with no cargo, which might indicate that slightly less fraction of the peptide molecules are reaching the TM state, when polar cargo is attached to the peptide inserting end.

While the equilibrium thermodynamics favor the binding and insertion of the pHLIP-cargo constructs, the slow kinetics could be limiting. Indeed, the most significant changes were observed in kinetics of the peptides insertion into a membrane when cargo was attached to the inserting end. The presence of a polar cargo slows the rate of the peptide's insertion several times, and intermediate states on the folding pathway are appeared, the similar changes were observed for the peptide with a charged inserting end (see previous paper). We carried out a detailed investigation of the kinetics of insertion for the pHLIP-2E variant (not described in the previous paper) and its conjugates with the biotin and biotin-Peg cargoes. First, we would like to outline a very important result: the kinetics of the pHLIP-2E's insertion into lipid bilayer in a result of pH drop could be very well described by the two-state model with no intermediates. Thus, as we predicted in the previous paper, in a simple case, the process of a polypeptide insertion/folding is an all-or-none transition. The pHLIP-2E is an excellent example of such case. When the polar cargo such as biotin or biotin-Peg is attached to the C-terminus of the pHLIP-2E, the process of insertion slows down about 400 times, and two intermediates appear on the folding pathway. We

assume, that the drop of pH leads, first, to the protonation (or partial protonation) of the Glu residues. As a result, the force directed toward a bilayer core ($\vec{F}_{in}$) is created (Figure 6). On the other hand, positively charged N-terminus and polar cargo at the C-terminus create a "pulling" forces ($\vec{F}_{out}$) that is directed out from the bilayer core, which prevent the propagation of the peptide into the membrane. We assume that more polar the cargo is, the higher the pulling force strength would be. The difference in the kinetics of insertion for the pHLIP-2E-bt and –btPeg is not significant. The slight difference is in the frequency factor, which is about two times lower for the pHLIP-2E-btPeg as compared to the pHLIP-2E-bt for the transition to the second intermediate on the folding pathway.

Our findings are very valuable for the design of new delivery agents for the direct translocation of a polar cargo across a membrane. There are several important conclusions we would like to make:

the simple case of the two-state folding model (insertion with no intermediates) is demonstrated by the membrane insertion of the pHLIP-2E peptide;

a polar cargo creates a "pulling" force, which might lead to the reduced affinity of a polypeptide-cargo to the membrane that is already at a neutral pH, thus the reduces the effective concentration of the cargo near the membrane surface;

it takes a significantly longer time for a polypeptide to adopt its final TM configuration, when a polar cargo is attached to the inserting end;

a polypeptide with cargo could be trapped in intermediates on the insertion/folding pathway;

there is no significant difference in the kinetics of a polypeptide insertion when cargoes of different polarity (Log *P* of -1.5 or -0.05) are attached to the peptide inserting end.

Finally, we can conclude that the pHLIP peptides with protonatable charged groups at the inserting end could be suited very well for the delivery of very toxic cargo molecules to have minimum efficiency of the translocation at a neutral pH (we have examples of such toxic cargo molecules). This is due to the fact that at a normal pH charged residues stays unprotonated preventing the peptide's insertion across a cellular membrane. However, the slow kinetics could be even more limiting for *in vivo* use, since the blood flow is very fast, and so there is not enough time for the equilibration to take place. Moreover, the 'trapping' in the intermediate state might occur and then no cargo translocation would happen. Therefore, if it is necessary to move as many cargo molecules as possible across a cellular membrane in a mildly-acidic environment, then the truncated pHLIP peptides with Glu protonatable residues could be much better fit. They would demonstrate a high rate and pKa of insertion. Thus, to facilitate the different delivery needs for the different applications i) the various peptides of the pHLIP family could be employed, and/or ii) the hydrophobicity of cargo could be tuned without affecting the cargo's ability to bind to its cellular target (10, 11).

ACKNOWLEDGMENT

This work was supported by a NIH grant CA133890 to OAA, DME, YRK. We thank Dhammika Weerakkody and Erin Jansen for the assistance in the spectral

measurements and the cargo conjugation to the peptides, respectively and Michael Anderson for the reading of this manuscript.

REFERNCES

1. Andreev, O. A., D. M. Engelman and Y. K. Reshetnyak. 2009. Targeting acidic diseased tissue: New technology based on use of the pH (Low) Insertion Peptide (pHLIP). *Chim. Oggi.* 27:34-37.

2. Andreev, O. A., D. M. Engelman and Y. K. Reshetnyak. 2010. pH-sensitive membrane peptides (pHLIPs) as a novel class of delivery agents. *Mol. Membr. Biol.* 27:341-352.

3. Andreev, O. A., A. D. Dupuy, M. Segala, S. Sandugu, D. A. Serra, C. O. Chichester, D. M. Engelman and Y. K. Reshetnyak. 2007. Mechanism and uses of a membrane peptide that targets tumors and other acidic tissues in vivo. *Proc. Natl. Acad. Sci. U. S. A.* 104:7893-7898.

4. Musial-Siwek, M., A. Karabadzhak, O. A. Andreev, Y. K. Reshetnyak and D. M. Engelman. 2010. Tuning the insertion properties of pHLIP. *Biochim. Biophys. Acta* 1798:1041-1046.

5. Reshetnyak, Y. K., O. A. Andreev, M. Segala, V. S. Markin and D. M. Engelman. 2008. Energetics of peptide (pHLIP) binding to and folding across a lipid bilayer membrane. *Proc. Natl. Acad. Sci. U. S. A.* 105:15340-15345.

6. Reshetnyak, Y. K., O. A. Andreev, U. Lehnert and D. M. Engelman. 2006. Translocation of molecules into cells by pH-dependent insertion of a transmembrane helix. *Proc. Natl. Acad. Sci. U. S. A.* 103:6460-6465.

7. Thevenin, D., M. An and D. M. Engelman. 2009. pHLIP-mediated translocation of membrane-impermeable molecules into cells. *Chem. Biol.* 16:754-762.

8. Vavere, A. L., G. B. Biddlecombe, W. M. Spees, J. R. Garbow, D. Wijesinghe, O. A. Andreev, D. M. Engelman, Y. K. Reshetnyak and J. S. Lewis. 2009. A novel technology for the imaging of acidic prostate tumors by positron emission tomography. *Cancer Res.* 69:4510-4516.

9. Reshetnyak, Y. K., L. Yao, S. Zheng, S. Kuznetsov, D. M. Engelman and O. A. Andreev. 2010. Measuring Tumor Aggressiveness and Targeting Metastatic Lesions with Fluorescent pHLIP. *Mol. Imaging Biol.* 107:20246-20250.

10. An, M., D. Wijesinghe, O. A. Andreev, Y. K. Reshetnyak and D. M. Engelman. 2010. pH-(low)-insertion-peptide (pHLIP) translocation of membrane impermeable phalloidin toxin inhibits cancer cell proliferation. *Proc. Natl. Acad. Sci. U. S. A.* 107:20246-20250.

11. Wijesinghe, D. D., D. M. Engelman, O. A. Andreev and Y. Reshetnyak, K. Tuning hydrophobicity of phallacidin cargo for improved translocation across plasma membrane by pH (Low) Insertion Peptide. *Submitted*.

12. Karabadzhak, A. G., D. Weerakkody, M. S. Thakur, D. M. Engelman, O. A. Andreev, V. S. Markin and Y. K. Reshetnyak. Membrane-associated folding: I. Spontaneous insertion/exit of a polypeptide into a lipid bilayer and formation of helical structure. *Submitted*.

13. Burstein, E. A., S. M. Abornev and Y. K. Reshetnyak. 2001. Decomposition of protein tryptophan fluorescence spectra into log-normal components. I. Decomposition algorithms. *Biophys J* 81:1699-1709.

14. Shen, C., R. Menon, D. Das, N. Bansal, N. Nahar, N. Guduru, S. Jaegle, J. Peckham and Y. K. Reshetnyak. 2001. The protein fluorescence and structural toolkit: Database and programs for the analysis of protein fluorescence and structural data. *Proteins: Struct., Funct., Bioinf.* 71:1744-1754.

15. Barrera, F. N., D. Weerakkody, M. Anderson, O. A. Andreev, Y. K. Reshetnyak and D. M. Engelman. New views of the pH-driven membrane insertion of the pHLIP peptide. *Submitted*.

16. Ferrari, M. 2005. Cancer nanotechnology: opportunities and challenges. *Nat. Rev. Cancer* 5:161-171.

17. Davis, M. E., Z. Chen and D. M. Shin. 2008. Nanoparticle therapeutics: an emerging treatment modality for cancer. *Nat. Rev. Drug Discovery* 7:771-782.

FIGURE LEGENDS

Figure 1. Three states monitored by the changes of fluorescence for pHLIP-cargo constructs. Three states of the pHLIP-4, -2 and -2E with the biotin and biotingPeg

cargoes monitored by the changes of the steady-state peptide fluorescence are presented (state I corresponds to the peptide-cargo in solution at pH8; state II corresponds to the peptide-cargo in the presence of POPC liposomes at pH8; state III corresponds to the peptide-cargo with the POPC, when the pH was dropped from 8 to 3.6 by addition of aliquot of HCl).

Figure 2. Three states monitored by the changes of CD for pHLIP-cargo constructs. Three states of the pHLIP-4, -2 and -2E with the biotin and biotingPeg cargoes monitored by the changes of the steady-state peptide CD are presented.

Figure 3. pH-dependent insertion into lipid bilayer of the membrane of the pHLIP-2-bt (***a***) and the pHLIP-2E-bt **(*b*)** is shown. The pKa of the transitions were found by the fitting of the curves with the Henderson–Hasselbalch equation. The fitting curves are colored in red.

Figure 4. Insertion into membrane of the pHLIP-4 and -2 without and with biotin cargo attached to the C-terminus. Insertion of the pHLIP-4-bt and pHLIP-2-bt is about 20 and 4 times slower than the insertion of the pHLIP-4 and pHLIP-2 with no cargo, respectively.

Figure 5. Insertion into membrane of the pHLIP-2E, -2E-bt and pHLIP-2E-btPeg at different temperatures, the Arrhenius plot. The kinetics of the fluorescence changes for the pHLIP-2E, -2E-bt, -2E-btPeg recorded at various temperatures are presented**.** The Arrhenius plots are shown on ***d***. The data were fitted by the Arrhenius equation (5). The fitting curves are colored in red.

Figure 6. Model of cargo translocation across a bilayer. The schematic presentation of the pHLIP-2E insertion into bilayer (***a***) and cargo translocation across a bilayer (***b***) in a result of the pH jump from 8 to 3.6. Circles represent approximate position of the protonatable carboxyl groups. The membrane distortion is shown by lipids with the darker headgroups.

TABLES

Table 1. Three states of the pHLIP-cargo constructs. The spectral parameters of the pHLIP-4, -2 and 2E conjugated to the biotin and biotin-Peg cargoes in the states I, II and III are presented. The parameters were obtained in the result of the analysis of the fluorescence and CD spectra shown on the Figure 1 and 2, respectively: the maximum position of the fluorescence spectrum λ_{max}, ***S*** – the normalized area under the spectra (normalization was done on the area under the spectrum in the state I); θ_{225} x 10^3, deg cm^2 $dmol^{-1}$ – the molar ellipticity at 225 nm.

		State I	State II	State III
Increase of A. for pHLIP-4 is 1.54 and 2.15 in states II and III				
pHLIP-4-bt	λ_{max} ***S*** θ_{225}	351.3 nm 1.0 -1.43	349.5 nm 1.23 -1.56	340.9 nm 1.48 -6.05
pHLIP-4-btPeg	λ_{max} ***S*** θ_{225}	351.5 nm 1.0 -1.44	349.7 nm 1.24 -1.76	341.3 nm 1.53 -6.04
Increase of A. for pHLIP-4 is 1.86 and 2.20 in states II and III				
pHLIP-2-bt	λ_{max} ***S*** θ_{225}	351.5 nm 1.0 -1.39	345.6 nm 1.51 -2.41	340.0 nm 1.96 -6.33
pHLIP-2-btPeg	λ_{max} ***S*** θ_{225}	350.3 nm 1.0 -0.99	347.5 nm 1.28 -1.43	338.6 nm 1.99 -5.05
Increase of A. for pHLIP-4 is 2.54 and 2.64 in states II and III				
pHLIP-2E	λ_{max} ***S*** θ_{225}	349.0 nm 1.0 -1.10	341.3 nm 2.54 -4.42	339.2 nm 2.64 -6.36
pHLIP-2E-bt	λ_{max} ***S*** θ_{225}	350.7 nm 1.0 -1.89	344.7 nm 1.71 -3.96	340.1 nm 2.41 -6.09
pHLIP-2E-btPeg	λ_{max} ***S*** θ_{225}	350.9 nm 1.0 -1.61	347.9 nm 1.50 -2.27	340.1 nm 2.26 -5.05

Temp	pHLIP-2E	pHLIP-2E-bt			pHLIP-2E-btPeg		
	t_1, s / k_1, s^{-1}	t_1, s / k_1, s^{-1}	t_2, s / k_2 s^{-1}	t_3, s / k_3 s^{-1}	t_1, s / k_1, s^{-1}	t_2, s / k_2 s^{-1}	t_3, s / k_3 s^{-1}
25ºC	0.20 / 4.55	0.20 / 5.00	1.59 / 0.57	82.4 / 0.012	0.20 / 5.00	3.7 / 0.24	86.0 / 0.0115
18ºC	0.28 / 3.25	0.28 / 3.57	2.67 / 0.34	95.0 / 0.010	0.28 / 3.57	5.8 / 0.16	103.9 / 0.0095
11ºC	0.34 / 2.68	0.34 / 2.94	4.04 / 0.22	110.0 / 0.009	0.34 / 2.94	7.0 / 0.13	125.0 / 0.0079
7ºC	0.39 / 2.33	0.39 / 2.56	5.21 / 0.17	124.4 / 0.008	0.39 / 2.56	10.0 / 0.09	133.3 / 0.0074

Table 2. Insertion at different temperatures Characteristic times (τ, sec), obtained in the result of the exponential fitting (eq. 1-2) of the fluorescence kinetics (transition from pH8 to 3.6) of the pHLIP peptides without and with cargo at different temperatures are presented. The rate constants (k, sec^{-1}) were calculated according to the eqs 3-4, these values were used to construct the Arrhenius plots (Figure 5*d*).

Table 3. **The activation energies and frequency factors**. The activation energy, E_a, and the frequency factor, ***A***, was calculated by the fitting of the Arrhenius plots (Figure 5*d*) by the Arrhenius equation (5).

	E_a, kcal/mol	*A*
pHLIP-2E	6.0	1.1×10^5
pHLIP-2E-bt	6.0 9.72 3.9	1.2×10^5 6.3×10^6 9.2
pHLIP-2E-btPeg	6.0 9.72 3.9	1.2×10^5 3.1×10^6 8.4

FIGURES

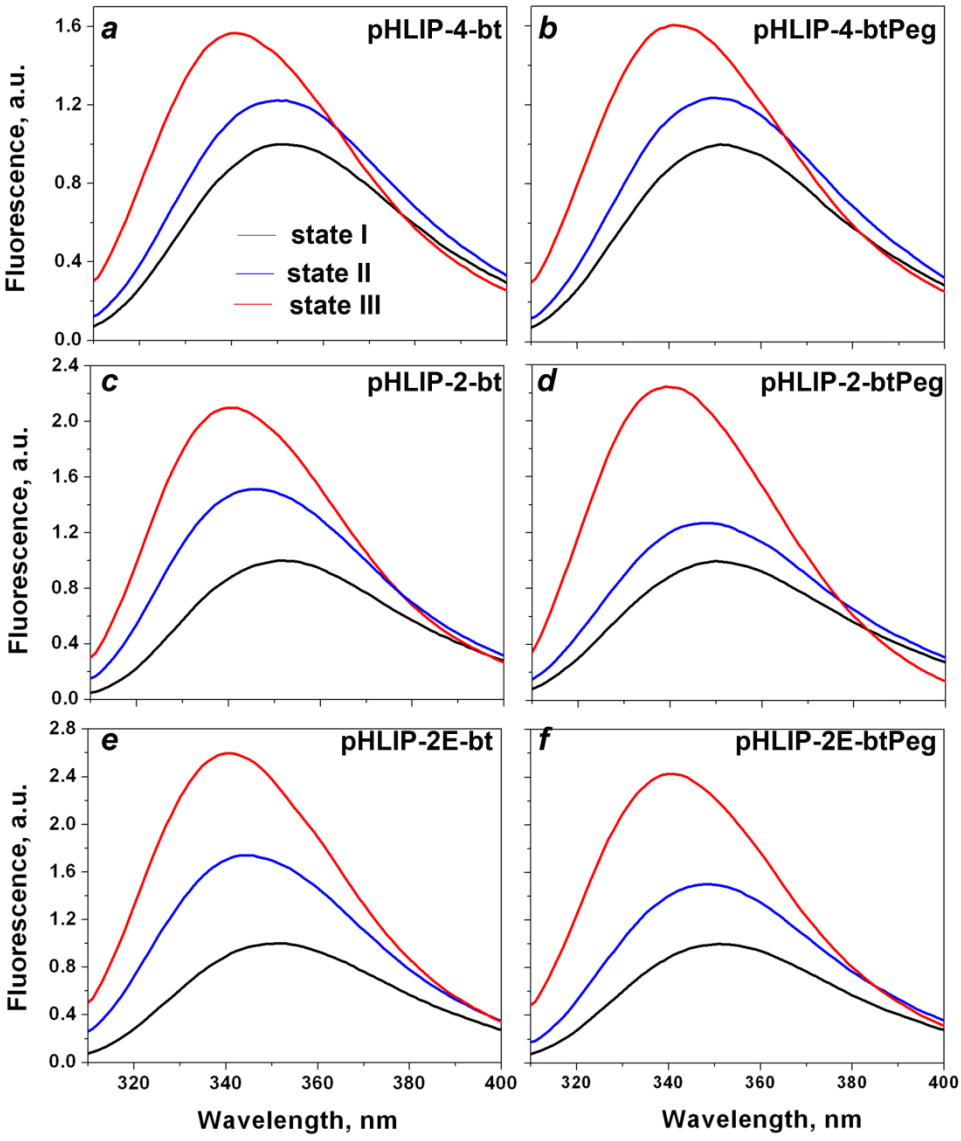

Figure 1

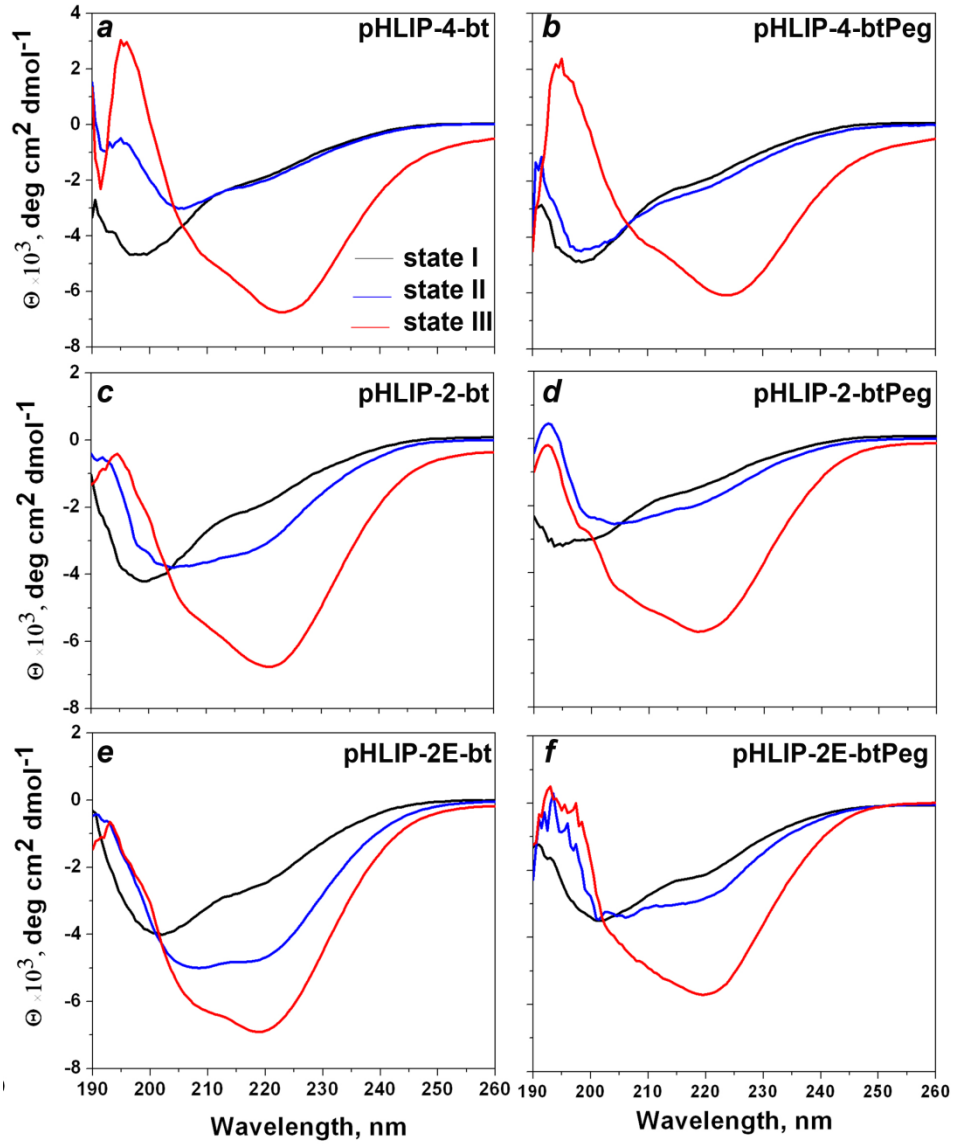
a
pHLIP-4-bt
b
pHLIP-4-btPeg
c
pHLIP-2-bt
d
pHLIP-2-btPeg
e
pHLIP-2E-bt
f
pHLIP-2E-btPeg
state I
state II
state III
Θ ×10^3, deg cm^2 dmol^-1
Wavelength, nm

Figure 2

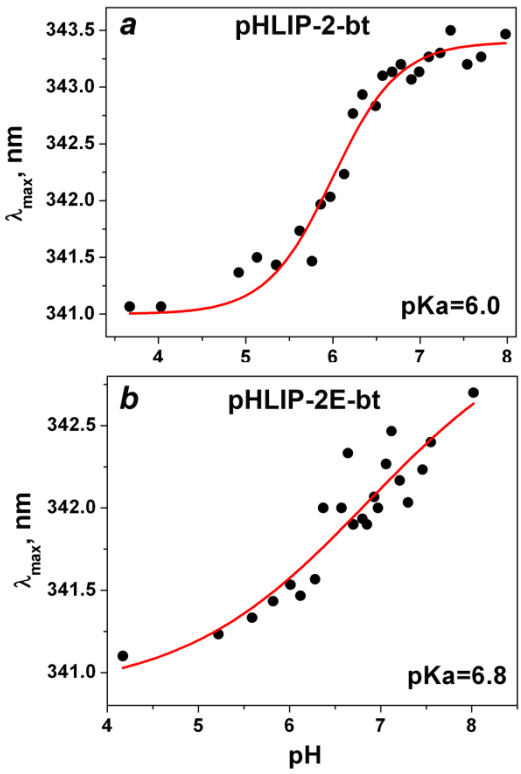

Figure 3

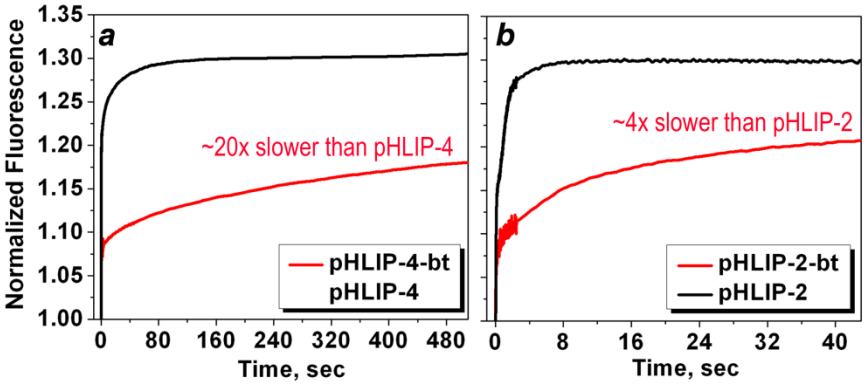
a
b
Normalized Fluorescence
1.35
1.30
1.25
1.20
1.15
1.10
1.05
1.00
~20x slower than pHLIP-4
~4x slower than pHLIP-2
pHLIP-4-bt
pHLIP-4
pHLIP-2-bt
pHLIP-2
0
80
160
240
320
400
480
8
16
24
32
40
Time, sec
Time, sec

Figure 4

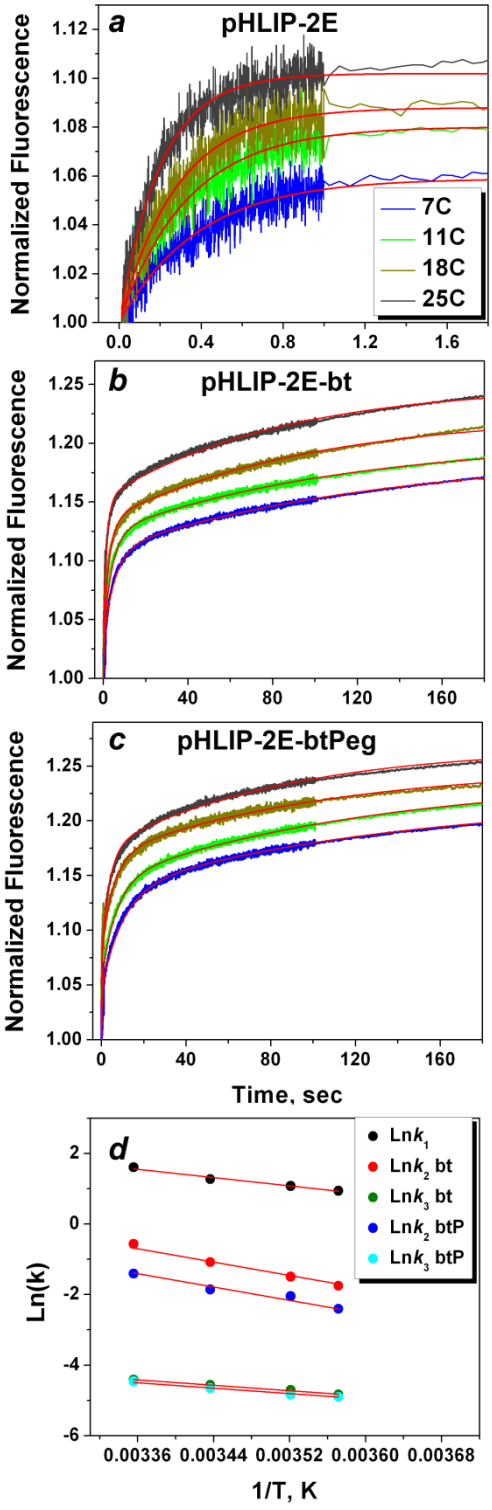
a
pHLIP-2E
Normalized Fluorescence
7C
11C
18C
25C
b
pHLIP-2E-bt
c
pHLIP-2E-btPeg
Time, sec
d
Ln(k)
1/T, K
Lnk1
Lnk2 bt
Lnk3 bt
Lnk2 btP
Lnk3 btP

Figure 5

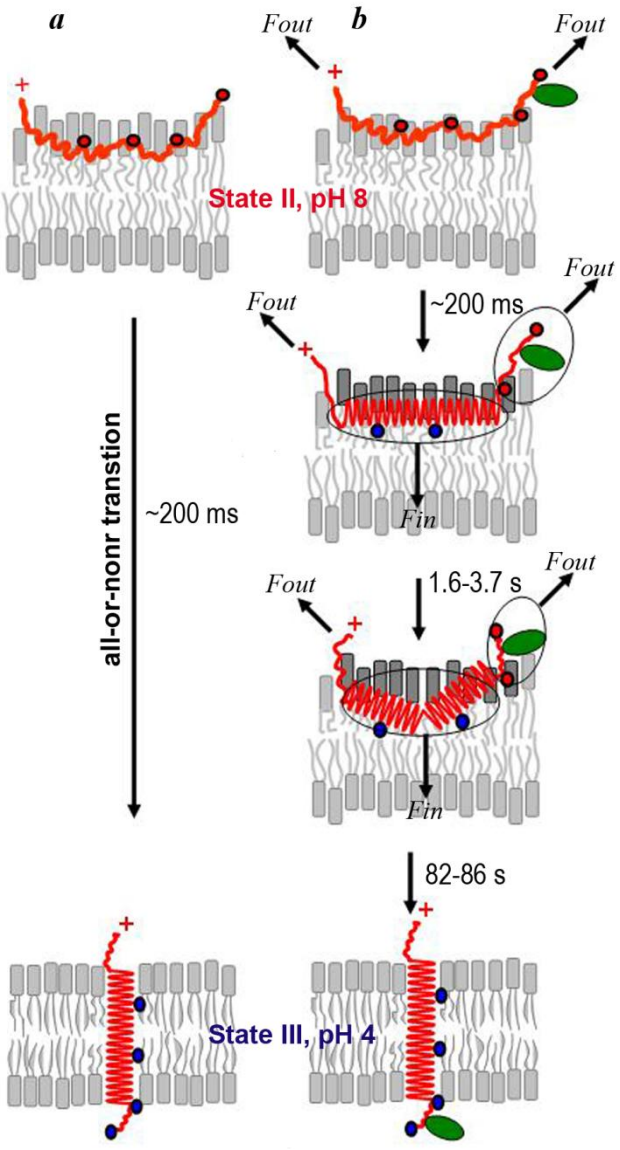
a
b
Fout
Fout
State II, pH 8
Fout
Fout
~200 ms
all-or-nonr transtion
~200 ms
Fin
Fout
Fout
1.6-3.7 s
Fin
82-86 s
State III, pH 4

Figure 6

APPENDIX 1

Two-State model

The two-state model is used to describe fast processes of folding of the pHLIP-2E variant, kinetic curves of which are fitted well by the single-exponential function. This model doesn't assume existence of intermediate states.

$$A \underset{k_1^-}{\overset{k_1}{\rightleftharpoons}} B \tag{1.1}$$

The transition from the state A to B is described by the differential equation:

$$\frac{d[A]}{dt} = -k_1[A] + k_1^-[B] \tag{1.2}$$

$$[A] + [B] = 1 \tag{1.3}$$

The variables *A* and *B* designate relative populations of the corresponding states. k_1 and k_1^- are the rates constant for the forward and backward reactions, respectively. We assume that initially all pHLIP molecules are in the state A and hence the initial conditions are:

$$A(0) = 1, B(0) = 0 \tag{1.4}$$

Exact solution of the differential equation 1.2 is the single-exponential function:

$$[A(t)] = \frac{k_1^-}{k_1+k_1^-} + \left(\frac{k_1}{k_1+k_1^-}\right) e^{-(k_1+k_1^-)t} \tag{1.5}$$

Some of the CD kinetic data were fitted by the single-exponential function:

$$S_{exp} = g_0 + g_1 \exp(-v_1 t) \tag{1.6}$$

where the characteristc rate v_1 expressed in a form of the rate constants is:

$$v_1 = k_1 + k_1^- \tag{1.7}$$

If we assume that equilibrium between the states A and B is strongly shifted to the right, meaning that $k_1 >> k^-_1$ and the difference between the rate constants at least an order of magnitude:

$$\frac{k_1}{k_1^-} \approx 10 \tag{1.8}$$

then we can estimate the rate of the forward reaction from the characteristic rate obtained in result of fitting of experimental data by single-exponential function:

$$k_1 \sim 0.91 v_1 \tag{1.9}$$

APPENDIX 2

Four-state model

The adequate fitting of the pHLIP-2E-bt and -btPeg kinetic data was achieved only by the three-exponential function. Therefore we introduced four-state model, which assumes existence of two intermediates:

$$\mathrm{A} \underset{k_1^-}{\overset{k_1}{\rightleftharpoons}} \mathrm{B} \underset{k_2^-}{\overset{k_2}{\rightleftharpoons}} \mathrm{C} \underset{k_3^-}{\overset{k_3}{\rightleftharpoons}} \mathrm{D} \tag{3.1}$$

The transitions in this system are described by the set of equations:

$$\frac{d[A]}{dt} = -k_1[A] + k_1^-[B] \tag{3.2}$$

$$\frac{d[B]}{dt} = k_1[A] - (k_1^- + k_2)[B] + k_2^-[C] \tag{3.3}$$

$$\frac{d[C]}{dt} = k_2[B] - (k_2^- + k_3)[C] + k_3^-[D] \tag{3.4}$$

$$[A] + [B] + [C] + [D] = 1 \tag{3.5}$$

The variables *A*, *B*, *C* and *D* designate relative populations of the corresponding states. We assume that initially all pHLIP molecules are in the state A and hence the initial conditions are:

$$A(0) = 1,\ B(0) = C(0) = D(0) = 0 \tag{3.6}$$

Finally the equilibrium will be reached and the equilibrium populations can be easily found by the graph technique:

$$A_0 = \frac{\leftarrow\leftarrow\leftarrow}{\leftarrow\leftarrow\leftarrow + \rightarrow\leftarrow\leftarrow + \rightarrow\rightarrow\leftarrow + \rightarrow\rightarrow\rightarrow} = \frac{k_1^- k_2^- k_3^-}{k_1^- k_2^- k_3^- + k_1 k_2^- k_3^- + k_1 k_2 k_3^- + k_1 k_2 k_3}$$

$$B_0 = \frac{\rightarrow\leftarrow\leftarrow}{\leftarrow\leftarrow\leftarrow + \rightarrow\leftarrow\leftarrow + \rightarrow\rightarrow\leftarrow + \rightarrow\rightarrow\rightarrow} = \frac{k_1 k_2^- k_3^-}{k_1^- k_2^- k_3^- + k_1 k_2^- k_3^- + k_1 k_2 k_3^- + k_1 k_2 k_3} \tag{3.7}$$

$$C_0 = \frac{\rightarrow\rightarrow\leftarrow}{\leftarrow\leftarrow\leftarrow + \rightarrow\leftarrow\leftarrow + \rightarrow\rightarrow\leftarrow + \rightarrow\rightarrow\rightarrow} = \frac{k_1 k_2 k_3^-}{k_1^- k_2^- k_3^- + k_1 k_2^- k_3^- + k_1 k_2 k_3^- + k_1 k_2 k_3}$$

$$D_0 = \frac{\rightarrow\rightarrow\rightarrow}{\leftarrow\leftarrow\leftarrow + \rightarrow\leftarrow\leftarrow + \rightarrow\rightarrow\leftarrow + \rightarrow\rightarrow\rightarrow} = \frac{k_1 k_2 k_3}{k_1^- k_2^- k_3^- + k_1 k_2^- k_3^- + k_1 k_2 k_3^- + k_1 k_2 k_3}$$

Solution of these equations is given by the three-exponential functions with the characteristic rates v_1, v_2, v_3 and it is rather cumbersome. We can assume that the first transition is very fast and the equilibrium is strongly shifted toward the state B, which means $k_1^- \approx 0$. Then

$$v_1 \sim k_1, \tag{3.8}$$

and

$$[A](t) = A_1 \exp(-v_1 t) \approx \exp(-k_1 t) \quad (3.9)$$

Remaining equations are:

$$\frac{d[B]}{dt} = k_1[A] - (k_1^- + k_2)[B] + k_2^-[C] \quad (3.10)$$

$$\frac{d[C]}{dt} = k_2[B] - (k_2^- + k_3)[C] + k_3^-[D] \quad (3.11)$$

$$[A] + [B] + [C] + [D] = 1 \quad (3.12)$$

To solve this set one can exclude *D*:

$$\frac{d[C]}{dt} = k_2[B] - (k_2^- + k_3)[C] + k_3^-(1 - [A] - [B] - [C]) \quad (3.13)$$

and then exclude *C*:

$$\frac{d^2[B]}{dt^2} + (k_2 + k_2^- + k_3 + k_3^-)\frac{d[B]}{dt} + (k_2^- k_3^- + (k_3 + k_3^-)k_2)[B] + [-(k_1 + k_2^- + k_3 + k_3^-)k_1 + k_2^- k_3^-]\exp(-k_1 t) - k_2^- k_3^- = 0 \quad (3.14)$$

Solution of this differential equation is given by

$$B = B_0 + B_1 \exp(-v_1 t) + B_2 \exp(-v_2 t) + B_3 \exp(-v_3 t) \quad (3.15)$$

with similar expressions for *C* and *D*. The first characteristic rate v_1 is given by the equation 3.8, and v_2 and v_3 are determined by:

$$v_i = -0.5(k_2 + k_2^- + k_3 + k_3^-) \pm \sqrt{0.25(k_2 + k_2^- + k_3 + k_3^-)^2 - k_2^- k_3^- - (k_3 + k_3^-)k_2} = -0.5(k_2 + k_2^- + k_3 + k_3^-) \pm 0.5\sqrt{(k_2 + k_2^- - k_3 - k_3^-)^2 - 4k_2^- k_3^-} \quad (3.16)$$

If we assume that the rates of consequent stages significantly decrease, i.e. $k_{2,}\,\bar{k}_2 >> k_{3,}\,\bar{k}_3$, then one can expand expression 3.16 into series and find solution in a simple form:

$$v_2 \approx (k_2 + k_2^-) + \frac{k_2^- k_3}{(k_2 + k_2^-)} \tag{3.17}$$

$$v_3 \approx \frac{k_2 k_3 + k_2 k_3^- + k_2^- k_3^-}{(k_2 + k_2^-)} \tag{3.18}$$

We can reasonably assume that the equilibrium (3.1) between the states B, C and D is strongly shifted to the right, meaning that $k_{2,} >> \bar{k}_2$ and $k_3 >> \bar{k}_3$. The difference should be at least an order of magnitude:

$$\frac{k_2}{k_2^-} \approx 10,\ \frac{k_3}{k_3^-} \approx 10 \tag{3.19}$$

and the rate constants are:

$$k_1 \sim v_1 \tag{3.20}$$

$$k_2 \sim \frac{v_2}{1.1} - \frac{v_3}{12.21} \tag{3.21}$$

$$k_3 \sim 0.991 v_3 \tag{3.22}$$